

NAVAL POSTGRADUATE SCHOOL ²

Monterey, California

AD-A246 836



DTIC
ELECTE
MAR 05 1992
S D

THESIS

STUDIES OF INTERMETALLIC GROWTH IN Cu-SOLDER
SYSTEMS AND
WETTABILITY AT SOLID-LIQUID INTERFACES

by

Raymond W. Martin

September, 1991

Thesis Advisor:

Professor I. Dutta

Approved for public release; distribution is unlimited

92 3 02 038

92-05310



REPORT DOCUMENTATION PAGE												
1a REPORT SECURITY CLASSIFICATION UNCLASSIFIED			1b RESTRICTIVE MARKINGS									
2a SECURITY CLASSIFICATION AUTHORITY			3 DISTRIBUTION/AVAILABILITY OF REPORT Approved for public release; distribution is unlimited.									
2b DECLASSIFICATION/DOWNGRADING SCHEDULE												
4 PERFORMING ORGANIZATION REPORT NUMBER(S)			5 MONITORING ORGANIZATION REPORT NUMBER(S)									
6a NAME OF PERFORMING ORGANIZATION Naval Postgraduate School		6b OFFICE SYMBOL (if applicable) Code 34	7a NAME OF MONITORING ORGANIZATION Naval Postgraduate School									
6c ADDRESS (City, State, and ZIP Code) Monterey, CA 93943-5000			7b ADDRESS (City, State, and ZIP Code) Monterey, CA 93943-5000									
8a NAME OF FUNDING/SPONSORING ORGANIZATION		8b OFFICE SYMBOL (if applicable)	9 PROCUREMENT INSTRUMENT IDENTIFICATION NUMBER									
8c ADDRESS (City, State, and ZIP Code)			10 SOURCE OF FUNDING NUMBERS									
			<table border="1"> <tr> <td>Program Element No</td> <td>Project No</td> <td>Task No</td> <td>Work Unit Accession Number</td> </tr> <tr> <td></td> <td></td> <td></td> <td></td> </tr> </table>		Program Element No	Project No	Task No	Work Unit Accession Number				
Program Element No	Project No	Task No	Work Unit Accession Number									
11 TITLE (Include Security Classification) STUDIES OF INTERMETALLIC GROWTH IN Cu-SOLDER SYSTEMS AND WETTABILITY AT SOLID-LIQUID INTERFACES												
12 PERSONAL AUTHOR(S) Raymond W. Martin												
13a TYPE OF REPORT Master's Thesis		13b TIME COVERED From To	14 DATE OF REPORT (year, month, day) September 1991	15 PAGE COUNT 81								
16 SUPPLEMENTARY NOTATION The views expressed in this thesis are those of the author and do not reflect the official policy or position of the Department of Defense or the U.S. Government.												
17 COSATI CODES			18 SUBJECT TERMS (continue on reverse if necessary and identify by block number)									
FIELD	GROUP	SUBGROUP	Cu-Pb solder, wettability, immersion-emersion technique									
19 ABSTRACT (continue on reverse if necessary and identify by block number) The metallurgical bond formed between tin-lead solder and the copper substrate is characterized by the formation of an intermetallic layer. The growth of the intermetallic layer is the result of competing mechanisms, growth of the intermetallic at the intermetallic/copper interface and its dissolution at the intermetallic/liquid solder interface. These were studied by determining the dissolution rates of the copper and the intermetallic compound. An experimental apparatus for the immersion-emersion tensiometric method, which can be used to determine immersion and emersion contact angles and surface tension, was set up and tested. This technique offers several advantages over the conventional sessile drop and tensiometric methods, and can be utilized to study wettability at solid-liquid interfaces.												
20 DISTRIBUTION/AVAILABILITY OF ABSTRACT <input checked="" type="checkbox"/> UNCLASSIFIED/UNLIMITED <input type="checkbox"/> SAME AS REPORT <input type="checkbox"/> DTIC USERS			21 ABSTRACT SECURITY CLASSIFICATION UNCLASSIFIED									
22a NAME OF RESPONSIBLE INDIVIDUAL I. Dutta, Professor			22b TELEPHONE (Include Area code) (408) 646-2581	22c OFFICE SYMBOL 69Du								

Approved for public release; distribution is unlimited.

Studies of Intermetallic Growth in Cu-Solder Systems
and
Wettability at Solid-Liquid Interfaces

by

Raymond W. Martin
Lieutenant, United States Coast Guard
B.S., U.S. Coast Guard Academy, 1984

Submitted in partial fulfillment
of the requirements for the degree of

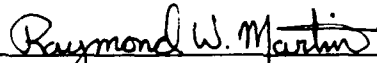
MASTER OF SCIENCE IN Mechanical Engineering

from the


NAVAL POSTGRADUATE SCHOOL


September 1991

Author:


Raymond W. Martin

Approved by:


I. Dutta, Thesis Advisor


Anthony Healy, Chairman

Department of Mechanical Engineering

ABSTRACT

The metallurgical bond formed between tin-lead solder and the copper substrate is characterized by the formation of an intermetallic compound layer. The growth of the intermetallic layer is the result of competing mechanisms, growth of the intermetallic at the intermetallic/copper interface and its dissolution at the intermetallic/liquid solder interface. These were studied by determining the dissolution rates of the copper and the intermetallic compound. An experimental apparatus for the immersion-emersion tensiometric method, which can be used to determine immersion and emersion contact angles and surface tension, was set up and tested. This technique offers several advantages over the conventional sessile drop and tensiometric methods, and can be utilized to study wettability at liquid-solid interfaces.



Accession For	
NTIS	CRA&I <input checked="" type="checkbox"/>
DTIC	TAB <input type="checkbox"/>
Unannounced	<input type="checkbox"/>
Justification	
By	
Distribution /	
Availability Codes	
Dist	Avail and/or Special
A-1	

TABLE OF CONTENTS

I. INTRODUCTION	1
II. BACKGROUND	4
A. SOLDERING IN ELECTRONICS	4
1. Basics	4
2. Known Joint Deficiencies	5
B. GROWTH OF INTERMETALLICS AT COPPER-TIN INTERFACE ..	6
1. Copper-Liquid Solder	6
2. Copper-Solid Solder	7
3. Nickel-Tin	9
C. MEASUREMENT OF CONTACT ANGLE AND SURFACE TENSION OF SOLID-LIQUID INTERFACES	10
1. Introduction	10
2. Intermetallic Wetting	11
3. Methods of Measuring Wettability - A Critical Appraisal	13
a. Sessile Drop Method	13
b. Wetting Balance or Tensiometric Method	14
c. Immersion-Emersion Tensiometric Technique	16

4. Immersion-Emersion Technique	18
III. OBJECTIVE OF THIS STUDY	29
III. EXPERIMENTAL APPARATUS AND METHODS	30
A. INTERMETALLIC FORMATION	30
1. Materials	30
2. Method	31
B. IMMERSION-EMERSION TENSIO-METRIC TECHNIQUE	39
1. Materials	39
2. Method	39
IV. EXPERIMENTAL RESULTS AND DISCUSSION	45
A. INTERMETALLIC FORMATION	45
1. Liquid Solder	45
2. Solid Tin	52
3. Review of Results	57
B. WETTABILITY MEASUREMENTS VIA THE IMMERSION- EMERSION TECHNIQUE	60
1. Procedure	60
2. Test Results	61

V. CONCLUSIONS AND RECOMMENDATIONS	69
A. INTERMETALLIC FORMATION AND COMPETING RATES OF DISSOLUTION	69
B. IMMERSION-EMERSION TENSIOMETRIC TECHNIQUE	70
LIST OF REFERENCES	72
INITIAL DISTRIBUTION LIST	74

I. INTRODUCTION

Soft-soldering is one of the oldest methods of metallic joinery. It is an inexpensive, reliable, simple, relatively low temperature technique. It is especially valuable in the electronics industry where high temperatures during manufacturing could damage the product. As electronics have become more complex the thermal stresses the soldered joints experience during the life of the product have greatly increased. Correspondingly, there has been much interest on the effects of these increased stresses on the reliability of the soldered joint. The scope of this work shall be confined to tin-lead solders on a copper substrate since this represents a large percentage soldering in today's electronic industry.

Tin-lead alloys are the most common soldering systems because their low melting temperatures and superior wetting properties. These alloys are characterized by a tendency to undergo structural change at the operating temperature, even if it is ambient temperature. Their low mechanical strength values, especially the low creep strength values, are related to this structural instability. Also these alloys exhibit a relatively fast solid-state reaction with elements such as gold and copper, producing intermetallic compounds. [Ref. 1: p. 141]

The intermetallic compounds between the solder and base metal, though necessary, adversely affect the mechanical joint. These compounds are generally brittle and have a coefficient of thermal expansion different than either the solder or the base metal. Joint

failure can occur due to thermal cycling or even during cooling after soldering [Ref. 2: p. 151]. Furthermore, the formation of a tin-rich intermetallic means that the adjacent tin-lead solder becomes lead-rich, hence lower intrinsic strength and ductility, [Ref. 1: p. 149]. It has also been shown that wettability is adversely affected by the intermetallic layer [Ref. 3: p. 49].

The growth mechanisms of the intermetallic layer and its morphology are of considerable interest in understanding the strength and reliability of soldered joints. This growth occurs while the solder alloy is still molten, at room temperature, during thermal cycling common in electronics and during reflow operations. The growth of the intermetallic layer is dependent on two competing mechanisms, i.e. the rate of formation of the intermetallic layer and the rate of dissolution of the layer in the liquid solder. The growth of the intermetallic is also affected by impurities and additives to the solder. The strength of the solder joint is directly affected by the characteristics of the intermetallic.

This work is comprised of two parts. The first part is a preliminary study of the differing diffusion rates governing the rate of intermetallic growth during the soldering phase when the solder is still liquid. The morphology of the intermetallic layer was also noted. In the second part, experimental apparatus to perform the immersion-emersion tensiometric technique of evaluating wettability was constructed and tested. This relatively new technique determines surface tension and contact angles at liquid-solid interfaces and offers several advantages over the conventional sessile drop and wetting balance or tensiometric methods. It is hoped that this method can be used to further understand the role of the intermetallic layer on the wetting of copper tin-lead systems

as the result of aging and reflow operations. Parameters such as impurity levels and percent lead content could also be varied and their effect on the wettability of the intermetallic layer could be studied.

II. BACKGROUND

A. SOLDERING IN ELECTRONICS

1. Basics

Soldering is the process of joining two metallic components with a molten filler metal (solder) having a melting temperature less than 450°C. In practice, the melting point is between 180 and 300°C [Ref. 1: p. 135].

For a satisfactory joint, wetting of solid metal surface by liquid metal is required. Wetting is indicated by the formation of layers of intermetallic compounds, for the copper lead-tin system they are Cu_6Sn_5 and Cu_3Sn . Mutual solid solubility or the formation of intermetallic compound layers between the solder alloy and the metal surfaces being joined is responsible for the reduction in the interfacial tension that leads to wetting. [Ref. 2: p. 150]

Interfacial tensions are related by the following equation:

$$\gamma_{\text{substrate/flux}} = \gamma_{\text{substrate/solder}} + \gamma_{\text{solder/flux}} \cos \theta \quad (1)$$

where θ is the contact angle of the solder on the substrate. When surface reactions occur the contact angle θ approaches zero to maintain the balance of forces. A contact angle of 180° represents no wetting of the surface, 90° represents wetting but no effective

spreading of the solder, and 0° is perfect wetting. An angle of 10° provides good solderability. Above 20° has been found to be indicative of a poor joint. [Ref. 2: p. 150]

The tin content of tin-lead alloys range from almost 100% down to 1%. The eutectic composition of the Sn-Pb (61.9% Sn-38.1% Pb or 61.9Sn-38.1Pb) has the lowest melting point. The physical properties of the solder change gradually with the tin-lead ratio. In practice, 60Sn-40Pb solder is the most widely used in the electronics industry. Tin concentrations greater than 60% are more expensive and therefore used less frequently. Lower tin concentrations are less expensive but below 50% tin wetting properties decrease thus solderability generally decreases with decreasing tin concentration. [Ref. 1: p. 137]

In tin-lead solder alloys, the tin is responsible for the wetting while the lead acts only as a diluent. The lead has been shown to affect the viscosity and the surface tension of the alloys but the effect of the tin-lead ratio on these properties does not correlate well with the physical behavior of the solders. [Ref. 2: p. 150]

2. Known Joint Deficiencies

The melting temperature, T_m , of most solders is rather low, between 180 and 200°C . The regular use of Sn-Pb solders at high homologous temperatures, T_o/T_m , means they experience structural changes at their operating temperatures, even if it is only room temperature. This structural instability results in low mechanical strength values. It also contributes to the fast solid-state reaction with copper thereby forming intermetallic compounds. [Ref. 2: p. 141]

The difference between the coefficients of thermal expansion, CTE, of the solder alloy and the substrate is the most common cause of solder joint failure. Because of this there are differing relative displacements across the joint. This results in strain being induced in the joint and when the temperature cycles fatigue results. [Ref. 4: p. 83]

The foregoing is rather simplistic. It is in fact much more complicated. The fatigue is driven by temperature therefore the mechanical properties of the solder change continuously during the fatigue cycle. Also because the peak operating temperature is often sufficiently close to the solder's melting temperature high temperature creep is an important deformation mode. The intermetallic compound layers may have different coefficients of thermal expansion from both the substrate and the solder alloy. Corrosion and chemical attack are two more factors which may affect the rate of fatigue. [Ref. 4: p. 83]

B. GROWTH OF INTERMETALLICS AT COPPER-TIN INTERFACE

1. Copper-Liquid Solder

Hagstrom and Wild [Ref. 5: p. 271] using direct measurement found intermetallic growth to be parabolic with time for short times but it reached a limiting value after 10 minutes. They did not look at the individual phases within the intermetallic.

Parent *et al.* [Ref. 6: p. 2572] using similar techniques found Cu_6Sn_5 reached a limiting value after 30 minutes and Cu_3Sn grew linearly with time with

no apparent limiting value. They found that the Cu_6Sn_5 grew in an irregular manner, consisting of a series of saw toothed protrusions which became more pronounced with time and temperature.

2. Copper-Solid Solder

Tu and Thompson [Ref. 7: p. 947], using Raman spectrometry, found Cu_6Sn_5 grew linearly with time and Cu_3Sn grew parabolically at the expense of the Cu_6Sn_5 .

Dehaven [Ref. 8], using *in situ* x-ray measurements, it was found the growth of Cu_6Sn_5 was linear with time initially and after a period of time became parabolic.

Davis *et al.* [Ref. 3: pp. 49-50] using direct measurements found the growth of both the total intermetallic layer and the Cu_3Sn to be parabolic with time.

Zakraysek [Ref. 9: p. 541], using scanning electron microscopy and x-ray probe analysis, found the intermetallics, Cu_6Sn_5 and Cu_3Sn , grow into the solder matrix and, at a slower rate, into the copper substrate. Insoluble and impurity elements concentrate ahead of the Cu_6Sn_5 /solder interface until growth is completed when all tin has been consumed. Diffusion continues until all intermetallic has been converted to Cu_3Sn . He states that the presence of insoluble alloying elements has a minor effect on the intermetallic growth rate. He also concluded that the tin content and the maximum exposure temperature have the greatest effect on the growth rates.

Warwick and Muckett [Ref. 10: p. 8] studied intermetallic growth over periods up to 12 years and at lower temperatures (20 to 170°C) than other

researchers. They found that when growth was plotted against the square root of storage time a straight line relationship was produced, i.e. parabolic growth, with a distinct "knee" near the origin. They found the growth rates of Cu_6Sn_5 and Cu_3Sn to be identical. The Cu_6Sn_5 growth was found to be preferential along certain lines. They believe this is due to faster intermetallic growth at the grain boundaries of the substrate. The morphology of the intermetallic layer differed depending on the method used to coat the copper substrate with tin or a solder alloy. When the tin was electroplated on the copper the growth appears uniform and angular. If the tin was reflowed in hot oil before ageing the growth is more irregular. Finally, if the tin was applied by hot dipping the growth appears as circular, columnar growth.

Klein Wassink [Ref. 1: p. 149] proposes that the intermetallic thickness can, in most cases, be approximated by the following parabolic relation:

$$\delta = k\sqrt{t} \quad (2)$$

in which:

δ = layer thickness after time t ,

k = growth constant at the temperature considered,

$$k = k_0 \exp\left(-\frac{Q}{RT}\right) \quad (3)$$

T = absolute temperature,

R = gas constant (8.32 J/mole.K or 1.04 eV/atom.K),

Q = activation energy of the growth,

k_0 = a constant, either in $\text{nm.s}^{-1/2}$ or $\mu\text{m.d}^{-1/2}$.

Klein Wassink noted the activation energy of growth of Cu_3Sn is about twice that of Cu_6Sn_5 . At room temperature, it is therefore predicted that the ratio of Cu_6Sn_5 thickness to Cu_3Sn thickness is about 500:1. This may explain why several researchers did not observe the presence of Cu_3Sn at lower temperatures. During growth the size of the Cu_6Sn_5 grains to increase. He found the morphology of the Cu_6Sn_5 to be columnar while the Cu_3Sn was more globular. [Ref. 1: pp. 155-157]

3. Nickel-Tin

Kang and Ramachandran [Ref. 11: p. 422] offer a thorough examination of intermetallic growth in liquid solder. Studying a nickel-liquid tin (Ni-Sn) system they found the intermetallic growth to be characterized by three stages; initial fast growth, followed by an intermediate stage of reduced growth, and recovery of fast growth in the final stage. Growth was found to be parabolic during the first and final stages. They state that once a uniform intermetallic layer grows at the Ni-Sn interface, the overall growth of the intermetallic, Ni_3Sn_4 , is determined by the motion of the two interfaces. The motion of the intermetallic-Sn interface is due to the dissolution of Ni directly from the intermetallic layer, because the solid-state diffusion of Ni through the intermetallic is believed to be very slow. The growth is reduced during the intermediate stage because of intermetallic dissolution into the tin bath but when the bath becomes saturated with nickel the dissolution of the intermetallic at the intermetallic/liquid interface slows and

the speed of the intermetallic growth increases. For short times they found the intermetallic to grow with planar boundaries while at the longer times the morphology became significantly faceted.

The manner in which these intermetallics form still requires understanding and may help explain the contradictory results obtained to date. Furthermore, the relationship between the selected diffusion parameters and the resulting appearance of the intermetallic layers is not yet clear [Ref. 1: p. 158].

C. MEASUREMENT OF CONTACT ANGLE AND SURFACE TENSION OF SOLID-LIQUID INTERFACES

1. Introduction

The possible use of the immersion-emersion tensiometric technique to study the wettability of the intermetallic compound offers several advantages over the conventional sessile drop and wetting balance or tensiometric methods. The method was developed by a French researcher Isabelle Rivollet [Ref. 12] and is relatively new. It offers the simultaneous measurement of the interfacial tension between the liquid and vapor phase, σ_{LV} , also known as surface tension and the contact angles of both immersion and emersion, θ_i and θ_e . This is done experimentally by dipping and withdrawing a solid cylinder in a liquid bath. Given these quantities the Young's contact angle, θ_Y , and work of adhesion, W_a , can be determined.

Young's contact angle is defined by the balance of forces at a solid-liquid-vapor triple line. The expression is:

$$\cos\theta_Y = \frac{\sigma_{SV} - \sigma_{SL}}{\sigma_{LV}} \quad (4)$$

where σ_{ij} are the interfacial tensions between two of the three phases and S, L, and V are the solid, liquid, and vapor phases.

The work of adhesion, W_a , is defined as the energy required to separate in a reversible manner a solid from a liquid [Ref. 12: p. 3179]. It therefore characterizes the interaction between liquids and solids. The expression is:

$$W_a = \sigma_{SV} + \sigma_{LV} - \sigma_{SL} \quad (5)$$

By combining equations (14) and (15) the following expression is obtained:

$$W_a = \sigma_{LV}(1 + \cos\theta_Y) \quad (6)$$

Therefore, it is seen that the immersion-emersion tensiometric technique provides the necessary information to determine σ_{LV} , θ_Y , and W_a .

2. Intermetallic Wetting

The wettability of the intermetallic compound has been investigated by several researchers. Past study has centered on the solderability of an aged copper tin-lead joint during reflow operations. Reflow soldering is the making of a joint by remelting

previously applied solder without applying additional solder. In practice, the term is used to describe any soldering process in which the solder and the heat are applied separately [Ref. 1: p. 541]. In the aged joint the intermetallic compound has grown, even possibly to the surface, thereby reducing or eliminating the quantity of unreacted solder available to melt during soldering.

Wassink [Ref. 1: p. 159] found that the Cu_6Sn_5 layer is less wettable than the previous tin or tin-lead coating. Molten solder will wet it using a strongly activated flux. An oxide layer forms on the intermetallic in air and has a strong effect on wetting. A layer of only 1.5 nanometers reduces the wettability below acceptable limits for soldering. At high temperatures the oxide layer on the intermetallic is smaller than would be present on either pure element alone. The thickness of the oxide layer that forms on both Cu_3Sn and Cu_6Sn_5 is about the same. It is from a few to 10 nanometers for temperatures of 175 to 250°C and times of 2 to 100 hours.

Davis *et al.* [Ref. 13: p. 72] indicated a 2 to 4 μm layer of intermetallic reduced solderability with the thickness of the unreacted coating having a less pronounced effect. More recent study by Davis *et al.* [Ref. 3: p. 49] has shown solderability to decrease when the thickness of the unreacted coating became less than about 5 μm . Therefore, with respect to solderability, thick intermetallic compound layers are acceptable if there is a sufficiently thick layer of unreacted coating above them.

Both of these studies examined coatings of tin and 60Sn-40Pb solder alloys. In the first study the solder coating was applied by electroplating while in the second study it was applied by electroplating and then reflowing the solder in oil. Warwick *et*

al. [Ref. 10: p. 10] has suggested that this difference in behavior is due to the different methods in coating but there is yet no theoretical explanation for this behavior.

3. Methods of Measuring Wettability - A Critical Appraisal

a. Sessile Drop Method

The sessile drop method is the most classical method for determining contact angles. The experimental apparatus consists of vacuum furnace fitted with two windows. Inside is a substrate of one metal with a pellet, known as a sessile drop, of another metal, the solder alloy, on it. A light source is placed in one window and the sessile drop's image is projected on a screen or photographed (Figure 1). As the drop melts contact angles are measured from the projected image or photographs. The actual experiment is conducted at constant temperature and the time-dependent variations of the contact angle θ are measured until a steady state value is observed.

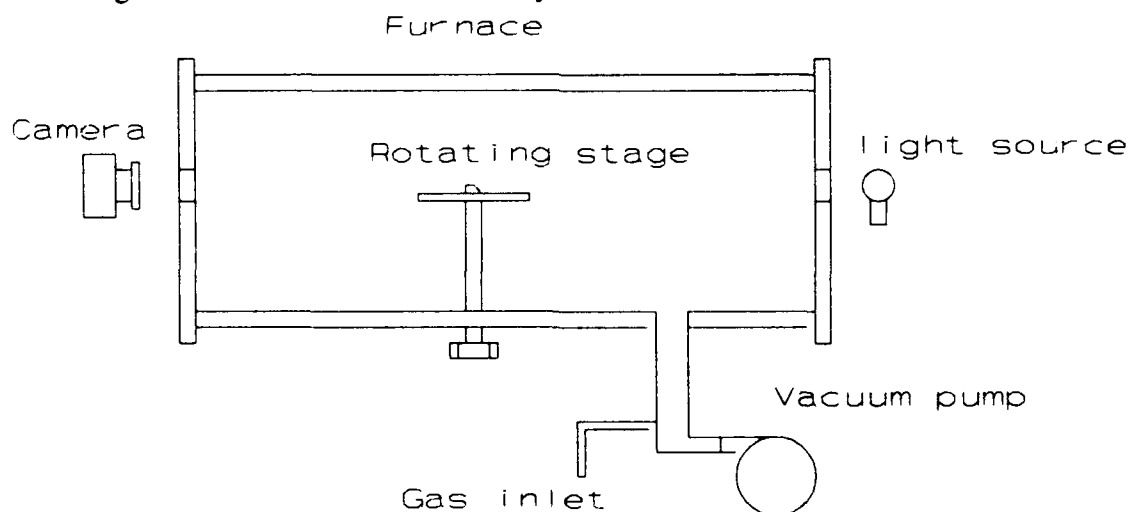


Figure 1 Sketch of sessile drop apparatus [Ref. 14: p. 245].

This method measures advancing contact angles and the advancing angle, θ_a , is always greater than Young's contact angle, θ_Y . This difference is due to the roughness of the substrate and several other factors which will be explained later [Ref. 14: p. 1798]. There are different techniques to produce advancing and receding angles and then determine θ_Y . They involve changing the volume of the drop or tilting the substrate but accomplishing this is difficult with liquid metals at high temperature in a vacuum or controlled atmosphere. [Ref. 12: p. 3179]

b. Wetting Balance or Tensiometric Method

The wetting balance method provides a versatile method of examining solderability. A metal specimen is suspended from a sensitive balance and immersed to a predetermined depth in a molten solder alloy at a controlled temperature. The forces of surface tension and buoyancy acting on the specimen are detected by the balance and a resultant plot of force as a function of time is produced on a strip chart recorder or a microcomputer. The plot is compared with a plot of a perfectly wetted specimen of the same nature and dimensions. After the specimen has been held at a specified depth for a given time, it is withdrawn from the bath (Figures 2 and 3).

In Figure 3 the speed of wetting can be seen as both the time required to change the upward force to a downward force and the time to achieve the steady-state wetting. It also shows plots for various degrees of wettability. The exact shape of the plot is dependent on parameters such as heat conductivity of the material, gas environment, type and amount of flux, and oxide layer thickness [Ref. 1: pp. 305-306].

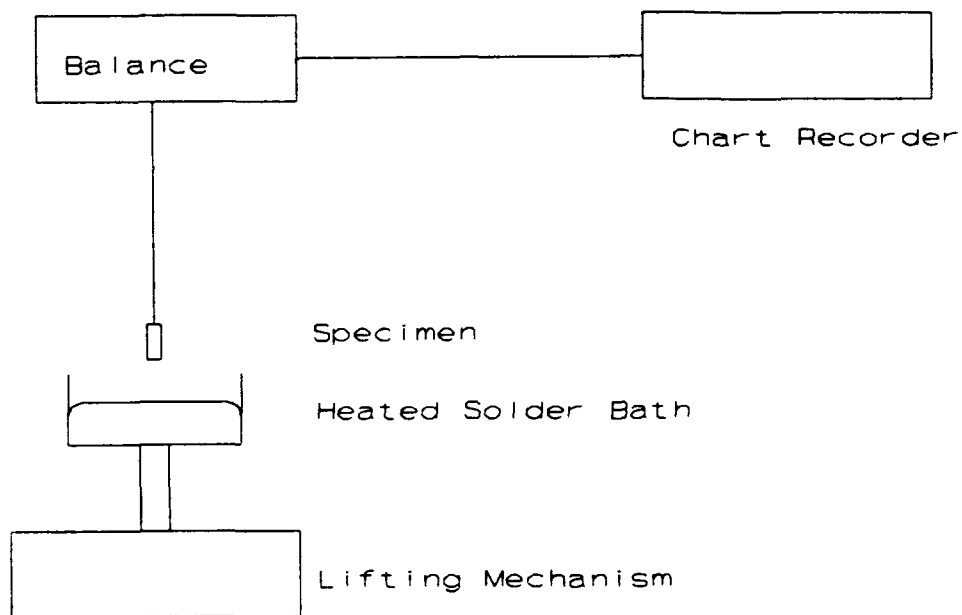


Figure 2 Sketch of wetting balance apparatus [Ref. 1: p. 305].

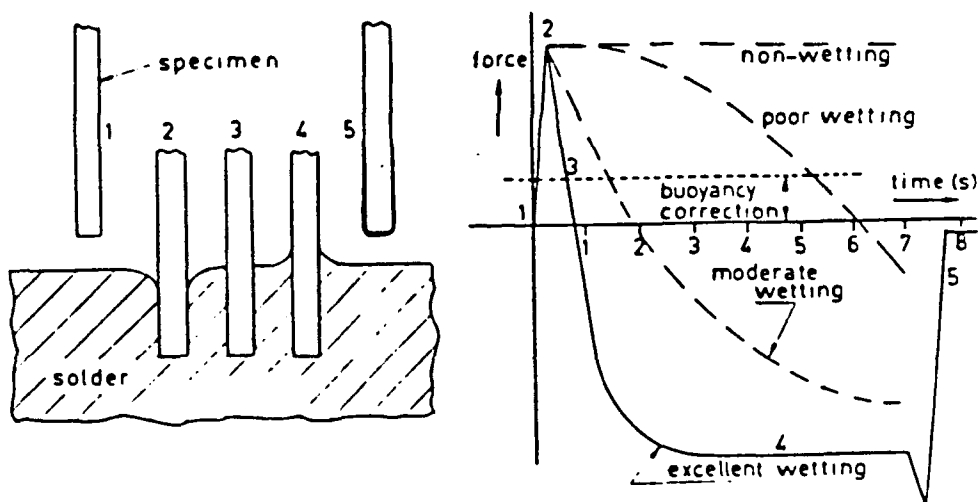


Figure 3 Left: Five situations of a wettable specimen. Right: Plot of forces on specimen as a function of time [Ref. 1: p. 305].

The contact angle, θ , can be measured optically if it is less than 90° . If θ is greater than 90° , the following equation is used provided the specimen cross-section is constant through its length in the vicinity of the meniscus:

$$\cos\theta = \frac{F}{p\sigma_{LV}} \quad (7)$$

where:

F = force at steady-state wetting condition, point 4 on Figure 3, for example,

p = perimeter length of immersed specimen,

σ_{LV} = surface tension of solder in contact with flux [Ref. 1: pp.304-308].

The major disadvantage of this method is it requires σ_{LV} to be known. Values of σ_{LV} have been tabulated for many metals and alloys but the experimental conditions used to measure the quantity will most likely be different from those during the use of the wetting balance. Differences can occur due to the temperature ranges used, contamination of the liquid by atmospheric elements or slight dissolution of the crucible holding the liquid or of the specimen itself. [Ref. 12: p. 3180].

c. Immersion-Emersion Tensiometric Technique

The two previous methods have several disadvantages. The measured contact angle, θ , obtained by the preceding two methods is always different than Young's contact angle, θ_Y . Also, the surface of the solid is never ideally chemically homogeneous

and/or smooth. This is due to original defects of the solid surface and/or other defects at the solid liquid interface. These two problems are attributed to three factors. First, the absorption-deabsorption of the liquid on the solid surface can affect the advancing and receding angles, θ_a and θ_r , by changing σ_{sv} . This is described as molecular hysteresis. Second, chemical heterogeneities on the solid surface can cause chemical hysteresis due to local variations of σ_{sv} and θ_{SL} . Finally, the roughness of the solid can cause topographical hysteresis by impeding the movement of the triple line as it moves on the solid. [Ref. 12: p. 3179]

Since these factors prevent direct measurement of θ_Y , the previous two methods attempt to approach it by measuring the advancing contact angle, θ_a , on the most ideal surface possible i.e. polished or monocrystalline [Ref. 12: p. 3179]. It has been found that if the R_a roughness, mean height value, of the specimen is less than 0.01 microns then the difference between θ_a and θ_Y is less than 8° [Ref. 14: p. 1798].

The primary aim of the immersion-emersion technique is determining the work of adhesion, W_a . To accomplish this σ_{LV} and the contact angles, θ_i and θ_r , are determined. The method involves measuring the variation in force as a function of the triple line towards the horizontal liquid surface, in other words, measuring the meniscus height and obtaining a numerical resolution of the Laplace equation giving the shape of the meniscus formed around a vertical solid cylinder [Ref. 12: p. 3180]. A description of the exact method and an analysis of its theoretical validity follows in the next section.

4. Immersion-Emersion Technique

The experimental apparatus is very similar in concept to the wetting balance. A solid circular cylinder is suspended from a balance. A vertical translation system is attached to a support that causes the cylinder to be immersed in and emersed from a liquid bath. The entire apparatus is located in furnace which permits operating in either a vacuum or a controlled atmosphere. Variations in the vertical force acting on the solid during its immersion and emersion are recorded as a function of time. Since the speed of the translation systems speed is known, the depth of immersion of the solid in the liquid is known. The output is to a strip chart recorder. [Ref. 12: p. 3180]

The technique is separated into two cases. The non-wetting case, θ_Y greater than 90° , will be presented first. The wetting case, θ_Y less 90° , will be covered later in this section. The non-wetting case is typical of ceramic-metal systems while the copper tin-lead system is wetting. The foundation of the following analysis is attributable to Rivollett [Ref. 15] unless otherwise noted.

The force, F , exerted on a solid partially immersed in a liquid is given by the following equation:

$$F = W_0 + W_m + \Delta \rho g z s \quad (8)$$

where:

W_0 = weight of the solid in the gas,

W_m = weight of the liquid meniscus,

$\Delta\rho$ = difference in density between the liquid and the gas,

g = acceleration due to gravity,

z = level of the base of the solid with respect to the flat horizontal surface of the liquid,

s = area of the base of the solid.

The weight of the meniscus, W_m , was demonstrated by Orr to be [Ref. 16]:

$$W_m = \sigma_{LV} p \cos \phi \quad (9)$$

where:

p = perimeter of a normal cross-section of the solid,

ϕ = the joining angle i.e. the contact angle at any instant.

The curve of variation of force as a function of depth of immersion is shown in Figure 4. The origin of the force is taken as the W_0 .

The following is an explanation of the various point on Figure 4:

A: solid contacts liquid,

A-B: meniscus forms progressively downward, velocity of the solid-liquid-vapor triple line with respect to the solid is zero,

C: $\phi = \theta_i$, meniscus shape remains constant, solid penetrates the liquid, variation of force from C to D due only to the buoyancy force, triple line moves at the velocity of the solid with respect to the liquid,

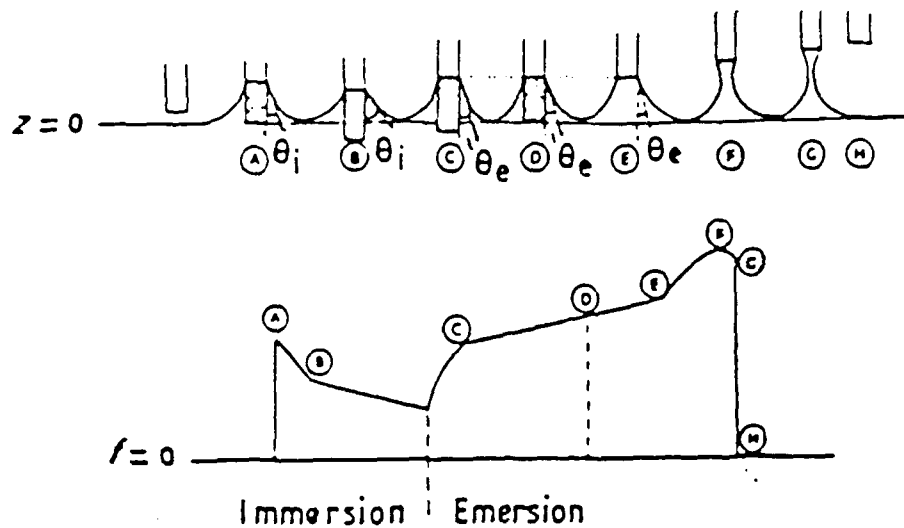


Figure 4 Common shape of the curve of variation of force, F , as a function of depth of immersion, z , for a non-wetting system [Ref. 12: p. 3181].

D: emersion begins, from D to E ϕ changes continuously from θ_i to θ_e .

E: $\phi = \theta_e$, from E to F the meniscus shape remains constant, change in force due only to buoyancy,

F: triple line is at the base of the solid,

F-G: ϕ goes from θ_e to $\theta_e - 90^\circ$,

G: finally, the meniscus falls off the solid.

For the wetting case, the experimental curve (Figure 5) is markedly different than the non-wetting case. First, θ_e occurs as soon as the solid touches the liquid. The speed of the triple line is not controlled by the solid-liquid speed but rather depends on θ_v and the viscosity of the liquid. Wetting has been found to occur in the order of

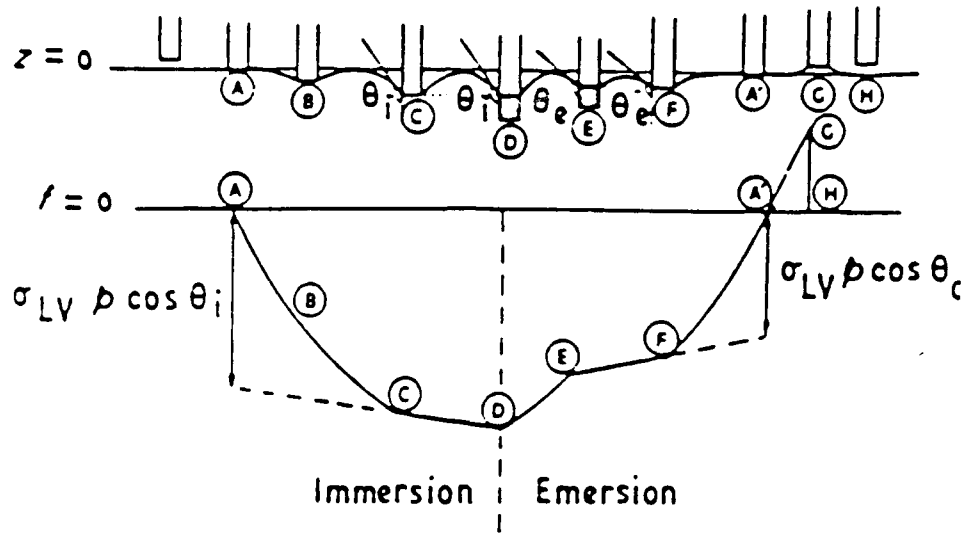


Figure 5 Common shape of the curve of variation of force, F , as a function of immersion depth, z , for a wetting system [Ref. 12: p. 3181].

thousandths of a second. Next, after immersion θ_i is reached at B but it is observed that θ_i is greater than θ_c . Finally, at the end of emersion ϕ goes through negative values from F to G. When the meniscus breaks off the solid $\phi = \theta_c - 90^\circ$. Prior to breaking off the force goes through a maximum value as a function of z . This value can be used to determine the surface tension directly and will be discussed later.

The surface tension is obtained from the non-linear portions of these curves (Figures 4 and 5). From the linear/non-linear intersection of these curves θ_i and θ_c are calculated. From equations (8) and (9), at each point along the curve from AC in Figure 6 for example, the product $\sigma_{LV} \cos \phi$ is known. Recall:

$$\sigma_{LV} \cos \phi = \frac{W_m}{p} \quad (10)$$

and

$$W_m = F - W_0 - \Delta \rho g z s \quad (11)$$

where W_0 is zero by convention and F and z are measured. The other equation relating σ_{LV} , ϕ , and z is the Laplace equation:

$$\Delta P = \sigma_{LV} \left(\frac{1}{r_1} + \frac{1}{r_2} \right) \quad (12)$$

where:

ΔP = pressure difference in and out of the liquid on each side of the surface,

r_1 and r_2 = the main curvature radii of the surface (Figure 6).

For the meniscus, ΔP is equal to the hydrostatic pressure:

$$\Delta P = \Delta \rho g z \quad (13)$$

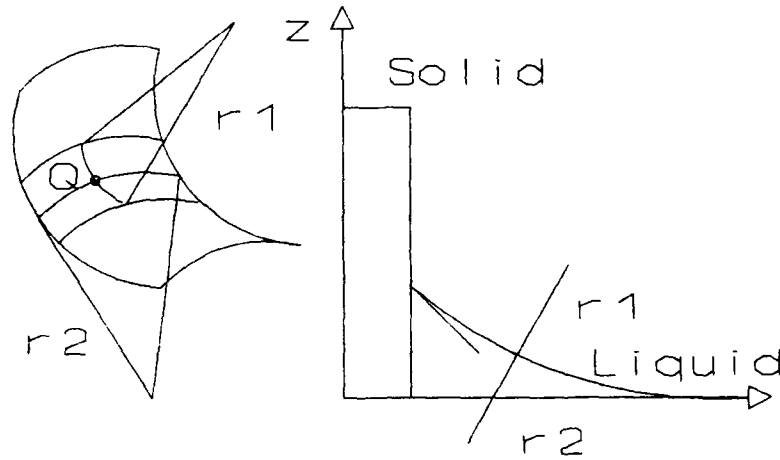


Figure 6 Left: Geometric quantities used to define the liquid surface shape. Right: vertical position z of any point Q on the surface and the joining angle ϕ of the liquid on the solid. [Ref. 12: p. 3182]

By combining equations (12) and (13), the following expression is obtained:

$$\sigma_{LV} \left(\frac{1}{r_1} + \frac{1}{r_2} \right) = \Delta \rho g z \quad (14)$$

To use this equation the values of r_1 and r_2 at any point Q (Figure 6) on the surface of the meniscus must be known. This is possible in only a limited number of cases. If the cylinder/meniscus shape is modelled as a vertical blade of infinite width, r_2 tends towards infinity. Therefore:

$$\frac{\sigma_{LV}}{r_1} = \Delta \rho g z \quad (15)$$

Previous researchers have found that from this version of the Laplace equation the following equation can be obtained for the height of the meniscus, z :

$$z = \sqrt{\frac{2\sigma_{LV}}{\Delta\rho g}(1 - \sin\phi)} \quad (16)$$

By combining equations (10) and (11), the following expression is obtained:

$$F = \sigma_{LV} p \cos\phi + \Delta\rho g z s = W_m + \Delta\rho g s z \quad (17)$$

Equations (16) and (17) are combined by eliminating ϕ and setting $s = 0$ and $p = L$ for the blade. This produces the following the final expression, σ_{LV} in terms of W_m and z . Furthermore, by the above derivation $W_m = F$. Therefore:

$$\sigma_{LV} = \frac{\Delta\rho g z^2}{4} + \frac{\left(\frac{F}{p}\right)^2}{\Delta\rho g z^2} \quad (18)$$

There are three methods of obtaining the value of σ_{LV} . Each method is more precise than the preceding method. First, equation (18) can be used for any point on the curve A-C of Figure 4 or curve E-F of Figure 5. For better results various points along these curves can be chosen. The best results are obtained by constructing a series of F vs. z curves for theoretical values of σ_{LV} . This is accomplished by choosing a σ_{LV} value and using equation (16) to obtain values of z for a series of ϕ values. Corresponding,

values of F are calculated using equation (17). The experimental curve is compared to the theoretical curves to obtain the experimental σ_{LV} .

The foregoing analysis was based on a solid blade of infinite width. Experimental results with a solid blade have differed from theory because of variations in the triple line level are caused by the corners of the blade. Therefore this analysis is only valid if the triple line belongs to a plane perpendicular to the vertical axis such as vertical cylinder of circular cross-section.

The contact angles, θ_i and θ_e , can determined from the experimental curve of F vs. z using the forces measured at points C and E of Figure 4 corrected for buoyancy (dashed lines). The equations for the corrected forces at A and E are:

$$F_A = \sigma_{LV} p \cos \theta_i \quad (19)$$

and

$$F_e = \sigma_{LV} p \cos \theta_e \quad (20)$$

Young's contact angle, θ_Y , is found from the following expression:

$$\theta_Y = \cos^{-1} \left(\frac{\cos \theta_i + \cos \theta_e}{2} \right) \quad (21)$$

where r is the Wenzel parameter, the ratio of the true area of the rough surface to the geometrical area.

Earlier it was stated that for the wetting case, θ less than 90° , σ_{LV} could be determined from the maximum force recorded during emersion. Another French researcher, Dominique Chatain [Ref. 17], proposed the following analysis.

As seen earlier, the force on the solid is:

$$F = \sigma_{LV} r \cos \phi + z \Delta \rho g s \quad (22)$$

and the relationship between z and ϕ is:

$$z = \sqrt{\left(\frac{2\sigma}{\Delta \rho g}\right)(1 - \sin \phi)} \quad (23)$$

If this is true then it is implied that at the point of maximum force:

$$\phi_{\max}'' < 0 \quad (24)$$

and

$$z_{\max}'' > \sqrt{\frac{2\phi}{\Delta \rho g}} \quad (25)$$

where the right side of equation (25) represents the maximum rise in height of the meniscus on the blade when $\phi = 0$. Chatain found that this analysis could not be rigorously applied because the blade is not of zero thickness. Experimentally it was found that at the point of maximum force:

$$z_{\max}^{\text{exp}} < \sqrt{\frac{2\sigma}{\Delta\rho g}} \quad (26)$$

$$\phi_{\max}^{\text{exp}} = 0 \quad (27)$$

and

$$F_{\max}^{\text{exp}} = \sigma_{LV}^{\text{exp}} p + \Delta\rho g z_{\max}^{\text{exp}} s \quad (28)$$

It is proposed the equation (28) can be used to directly calculate σ_{LV} for the wetting case given the two measured quantities F and z_{\max} . [Ref. 17]

Examination of equation (28) reveals forces due to both the weight of the meniscus and buoyancy. Recalling Rivollet's analysis, the maximum force occurred when the cylinder was no longer immersed in the liquid but was rather "stretching" the liquid. Chatain found that even at the condition of maximum force some of the solid was immersed in the liquid. This is because his study used a plate of finite width. The corners of the plate cause variations of the triple line level. If he had used a cylinder

these variations would not exist and the triple line would be level. Therefore, Rivollet's analysis would be correct. Figure 7 illustrates the two ideas.

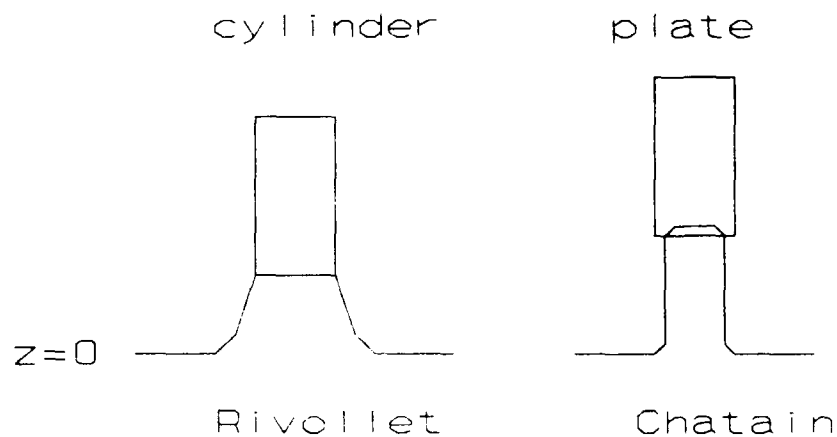


Figure 7 Meniscus shape at maximum force.

Based on this analysis, for a wetting system, $z = 0$ at the condition of maximum force and equation (28) becomes:

$$\sigma_{LV} = \frac{F_{\max}^{\text{exp}}}{p} \quad (29)$$

This equation is used to calculate σ_{LV} for a solid cylinder used in a wetting system.

III. OBJECTIVE OF THIS STUDY

The goal of the first part of this work is to better understand the mechanisms involved in the formation of the intermetallic compound layer between liquid tin-lead solder and a copper substrate. Specifically, the competition between intermetallic growth at the intermetallic/metal interface and the dissolution at the intermetallic/liquid boundary has been investigated. Various soldering temperatures and times will be studied. The effect of solder composition will also be considered. During the course of this work the morphology of the intermetallic will also be examined.

The goal of this work is to construct and test experimental apparatus needed to perform the immersion-emersion tensiometric technique. In particular, analysis of a wetting system will be studied to determine the feasibility of using the method to examine the wettability of the intermetallic compounds Cu_6Sn_5 and Cu_3Sn .

III. EXPERIMENTAL APPARATUS AND METHODS

A. INTERMETALLIC FORMATION

1. Materials

To help understand the relative rates of these two mechanisms the dissolution of copper wires and Cu_6Sn_5 coupons in liquid tin and 61.9Sn-38.9Pb solder baths were studied. The copper wire used was 20-gauge with a purity of 99.90%. The solder baths were made with tin pellets and lead powder with purities of 99.5%. The same tin was used in the Cu_6Sn_5 coupons and the copper purity was 99.5%.

The Cu_6Sn_5 coupons were manufactured in the lab. The tin pellets and copper powder were combined in the correct stoichiometric ratio, 60.7 wt. % tin and 38.3 wt. % copper, obtained from the copper-tin phase diagram. The mixture was placed in a 9 mm diameter Vycor tube. The tube was evacuated to 10^{-5} torr and sealed. Placing the pellets above the powder in the tube prevented the powder from being lost in the vacuum system. The sealed tube was placed in a 1200°C furnace until the mixture was completely liquid. It was then removed, shaken, and placed back in the oven. When it was liquid again it was removed from the oven, solidified, and annealed for 3 days in a 350°C furnace. The final chemical composition of the solid was checked using x-ray diffactometry. Purity was approximately 90% Cu_6Sn_5 and the remainder was unreacted tin and copper. The cylindrical solid was cut into rectangular coupons using a slow speed diamond saw.

2. Method

The method involved the use of a thermostatically controlled bath with the solder. The period of time the specimen was in the bath and the solder bath temperature were varied. In this work the two solder bath compositions were examined at three different temperatures and at least five different lengths of time.

The experimental procedure consisted of dipping copper wires or Cu_6Sn_5 coupons in a thermostatically controlled bath of liquid solder for various lengths of time. Upon removal they were quenched and prepared for observation using several different methods. Scanning electron microscopy was used to view and make measurements of the specimens.

Approximately 40 grams of liquid solder was held in a VYCOR glass crucible. The crucible was in thermostatically controlled bath of liquid. Temperature was recorded by a thermocouple in the solder. Temperature was maintained at $\pm 2^\circ\text{C}$ during the specimen dipping. The solder was changed after five specimen dippings to minimize the concentration of dissolved copper [Ref. 18: p. 553]. Research has shown that when the copper concentration reaches 0.2% by weight the diffusion process is self-limiting [Ref. 2: p. 184]. The copper specimens were 1.5 inches long and 508 μm in diameter. The Cu_6Sn_5 varied in size but averaged 1 mm thick, 6 mm wide, and 25 mm long. The specimens were degreased for 30 seconds in a 6 molar hydrochloric acid solvent, rinsed in distilled water, air dried, and fluxed using a commercial resin flux prior to dipping to ensure wetting [Ref. 18: p. 72]. Specimens were quenched in water immediately after removal from the liquid solder.

Specimens were prepared using several different methods depending on the type of viewing desired. To examine the surface morphology of the Cu_6Sn_5 formed on the copper wires the outer unreacted layer of solder was etched off. This was done by immersing the specimen in a solution of 50 g of sodium hydroxide, NaOH , and 35 g of nitrophenol, $\text{C}_6\text{H}_5\text{NO}_3$, in 1 liter of distilled water. The solution was heated to 75°C and ultrasonically agitated. [Ref. 1: p. 158]

After complete removal of the tin, indicated by a uniform matte gray appearance, the specimen was washed in warm distilled water and dried in warm air using acetone [Ref. 19: p. 451]. The specimen was then placed in the scanning electron microscope (SEM) immediately for viewing of the surface. The surface was found to quickly oxidize in air. Representative photographs were taken of the surface at approximately the same position on each sample (Figure 8).

All specimens were cold mounted vertically using spring clips so that their cross-section could be viewed in the SEM. Multiple specimens were placed in each cold mount. Specimen preparation consisted of grinding on progressively finer sand paper down to 600 grit. Then they were polished on a $6\text{-}\mu\text{m}$ diamond paste polishing wheel at 200 rpm. Final polishing was on a $0.05\text{-}\mu\text{m}$ alumina wheel. Specimens were cleaned using water and dried with warm air [Ref. 19: p. 400].

This method prevents steps from forming on the surface of the specimen due to the differences in hardness between the copper, tin, and Cu_6Sn_5 . These steps make it impossible to view the interfaces between the phases. Next the specimens were placed

under vacuum to draw any liquid out of the crevices between the mounting resin and the spring clips.

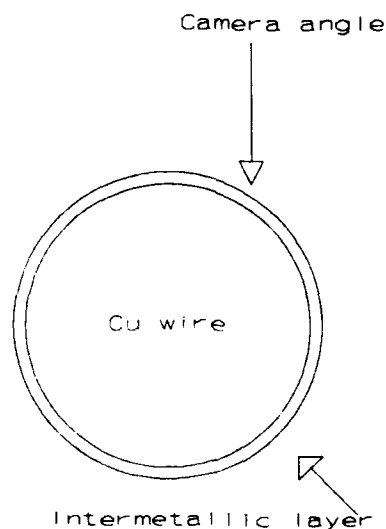


Figure 8 Location of Cu_6Sn_5 viewed on copper wires.

To view the intermetallic formed on the wires which had not been stripped of unreacted tin, specimens were mounted, prepared and then etched to darken the unreacted tin. The etchant procedure was a 10 second swab with 60% H_2O_2 -40% NH_4OH followed by a 10 second swab with 2% HNO_3 -98% alcohol [Ref. 9: p. 538].

Finally, for viewing in the SEM, they were plated with a thin film of gold in a vapor deposition unit. For viewing the cross-section of the wires, it was found to be preferable not to strip off the unreacted tin. Viewing the thin intermetallic layer next to the mounting resin proved difficult because the resin would heat up and flow onto the area being viewed. Etching the unreacted tin proved effective for optical microscopy but was of minimal value in the SEM. Backscattered electron imaging proved to be the best way to view the cross-section of the copper wire.

In the SEM measurements were made of the diameter remaining of the copper and thickness and width remaining of the Cu_6Sn_5 coupon. Multiple measurements were taken on each specimen and an average was obtained. For the diameter measurements were 20° apart and for the thickness and width they were equidistantly spaced. The thickness of the intermetallic formed was also measured though it was difficult because of the irregular growth. Fifteen measurements were taken around the perimeter of each specimen. Maximum and minimum thicknesses were also noted.

It was desired to plot the two dissolution rates against time and temperature for the two solder compositions considered. This would allow comparison of the competing diffusion rates. This proved to be problematic since the size and shape of the copper and the intermetallic coupons differed. The solution used was to compare the loss of radius of the copper wire, ΔR , to an effective loss of radius of the rectangular coupon, ΔR_{eff} .

The concept relating a loss in area of a rectangular coupon to an effective loss of radius by a circular cylinder is based on the following analysis. First, the flux of mass out of the rectangular bar is equal to the flux out of the cylinder. Next, it is assumed that the mass lost out the bottoms of the circular rod and rectangular cylinder is negligible in comparison to that lost out the side. Also, it is assumed that there is no type of convective mass transport occurring at the surface of the bar or rod.

The volume of mass lost by a cylinder, ΔV_c , is defined as:

$$\Delta V_c = \pi(R^2 - (R - \Delta R)^2)L \quad (30)$$

therefore,

$$\Delta V_c = \pi(-\Delta R^2 + 2R\Delta R)L \quad (31)$$

finally,

$$\Delta V_c = 2\pi R\Delta RL \quad (32)$$

in which:

R = initial cylinder radius,

ΔR = radius lost by cylinder,

L = length of cylinder in solder bath.

The quantity ΔR^2 is considered negligible.

The volume of mass lost by the rectangular rod, ΔV_r , is defined as:

$$\Delta V_r = TWL - (T - \Delta T)(W - \Delta W)L \quad (33)$$

therefore,

$$\Delta V_r = -\Delta T \Delta WL + \Delta WTL + \Delta TWL \quad (34)$$

finally,

$$\Delta V_r = (T \Delta W + \Delta TW)L \quad (35)$$

in which:

T = initial thickness,

W = initial width,

L = length of rod in solder bath,

ΔT = thickness lost by rod,

ΔW = width lost by rod.

The quantity $\Delta T \Delta W$ was considered negligible.

The volume of mass lost and flux of mass out of the perimeter of the cylinder and rod are related by the following equations:

$$\rho \frac{\Delta V_c}{\Delta t} = J 2\pi R L \quad (36)$$

and

$$\rho \frac{\Delta V_r}{\Delta t} = J(2TL + 2WL) \quad (37)$$

in which:

ρ = density of cylinder or rod,

Δt = time of immersion in solder bath,

J = flux (mass per area per time)

Since flux is constant equations (36) and (37) can be equated.

$$\frac{\Delta V_c}{2\pi R L} = \frac{\Delta V_r}{2(TL + WL)} \quad (38)$$

Substituting in equations (30) and (31) into equation (12) produces a relationship for the loss of area by a rectangular rod as an effective loss of radius of a circular cylinder, ΔR_{eff} .

$$\Delta R_{eff} = \frac{T\Delta W + \Delta TW}{2(T+W)} \quad (39)$$

This effective change in radius was used to compare the Cu_6Sn_5 dissolution rate, $\Delta R_{eff}/dt$, with the copper dissolution rate, $\Delta R/\Delta t$, in the two solder compositions at three different solder bath temperatures.

This analysis was tested by comparing the dissolution rate of copper wires to the effective dissolution rate of copper coupons of approximately the same dimensions as the Cu_6Sn_5 coupons. The results are listed in Table I. The effective dissolution rate was found to be less than twice the copper wires dissolution rate. This may be due to the simplifying assumptions used in its derivation.

Table I Comparison of copper dissolution rates with the derived effective dissolution rates. 100% tin bath at 270°C was used.

Time in solder bath sec	dR/dT Cu wires μm/sec.	dR _{eff} /dT Cu coupons μm/sec.	% difference
120	0.1233	0.1923	56.0
180	0.1440	0.2430	68.7
240	0.1393	0.2541	82.4

B. IMMERSION-EMERSION TENSIO-METRIC TECHNIQUE

1. Materials

The copper cylinders used were 6 mm in diameter. Their purity was 99.9%. Solder bath components were from the same stock used in the dissolution experiments. The inert gas used was argon.

2. Method

The apparatus required for the immersion-emersion method consisted of a precision microbalance from which a solid cylinder was hung. A crucible with the liquid solder bath was connected to a vertical translation system. The bath was moved up to the solid and the solid was immersed and emersed. The bath was located in a furnace with a controlled atmosphere. This allows the study of liquid metals. Changes in the vertical force acting on the 'solid were recorded on a strip chart recorder with respect to time. Actually, the microbalance recorded changes in mass which were easily converted to changes in force and time was converted to depth of immersion since the translation speed of the bath was known and constant. The final output was a curve of variation of force as a function of depth of immersion.

A MELLE tube furnace with an 18 inch heated length, 4 inch diameter, and maximum temperature of 1200°C was used. A EUROTHERM temperature controller used a thermocouple located near the crucible to maintain constant temperature.

The microbalance used was a CAHN 2000 analog recording balance. It has dual capacity of 1.5 gm and 3.5 gm and can record weight changes of 150 mg and 750

mg, respectively. Sensitivities are 0.1 μ g and 1.0 μ g. It was placed in a vacuum bottle that allows use with vacuum or controlled atmosphere systems. Extension wires were constructed out of nichrome wire (Figure 9).

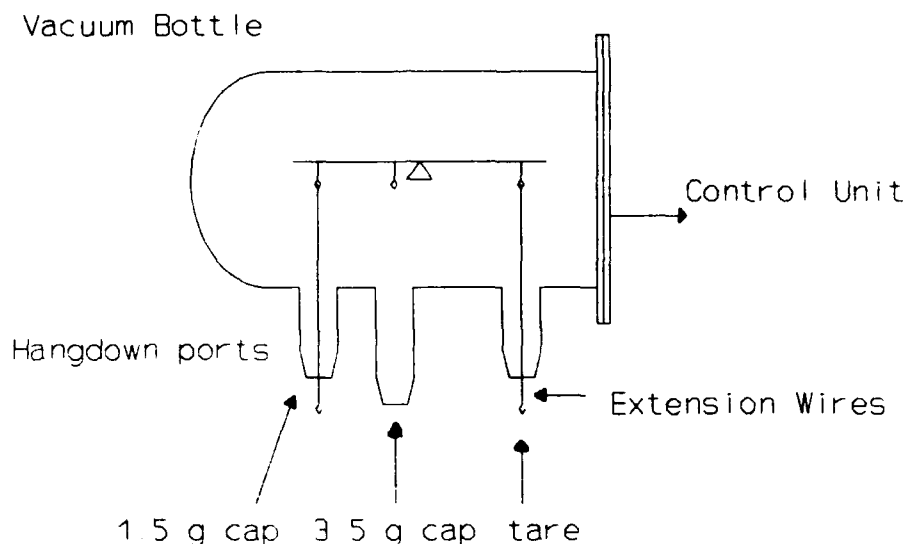


Figure 9 Microbalance schematic.

The crucible was a COORS silica crucible 38 mm in diameter. It was mounted on a movable stage suspended in the furnace. The stage was made of machinable ceramic and it moved vertically on three ceramic rods. Stainless steel collars held the apparatus together because the rods were not machinable (Figure 10). A ceramic beam connected the movable stage to the translation motor below the furnace. A slow speed motor turned a threaded shaft in and out of the beam. Translations speeds between 0.5 mm/min and 1.8 mm/min. were possible. Motion was very smooth to prevent

disturbing the liquid bath. The vertical speed of the movable stage was calibrated with respect to the voltage setting on the motor controller (Figure 11).

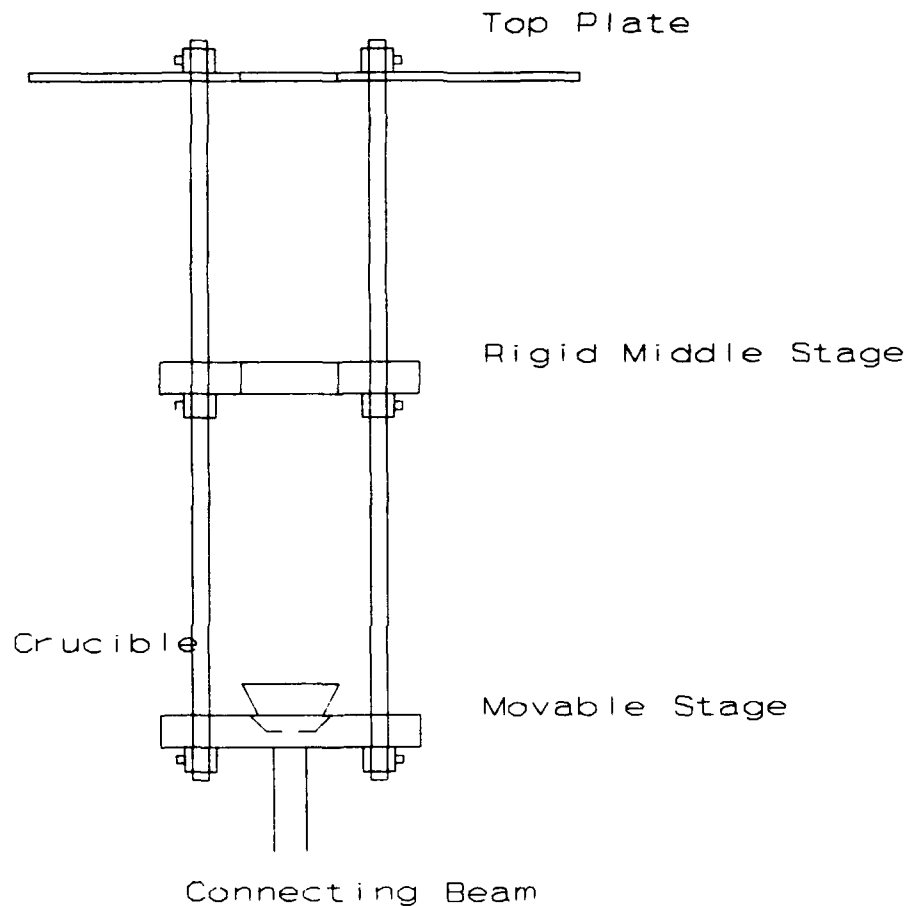


Figure 10 Movable stage.

Figure 12 illustrates the entire apparatus. Apparatus was set on a wall mounted stand that allowed the balance to be moved horizontally so both hangdown ports could be used. The balance also had approximately 8 inches of vertical travel. It was

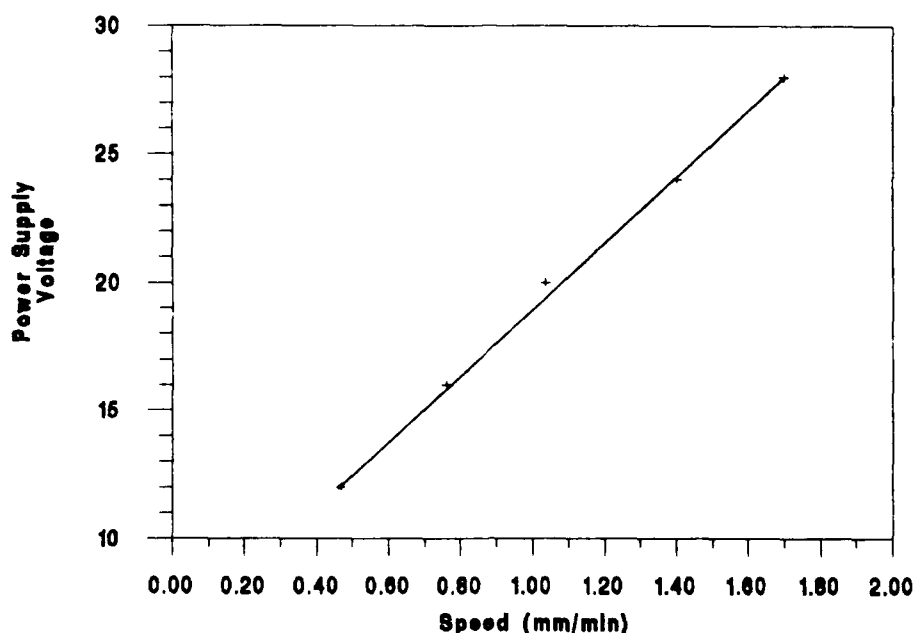


Figure 11 Calibration chart for translation motor.

also hinged to allow horizontal movement. Hangdown ports had glass covers. A 28 inch hangdown tube extended into the furnace. Inert gas could be flowed through this tube.

Operation of the apparatus was simple in principle. The balance is calibrated and zeroed in accordance with the manufacturer's instructions. The crucible is filled with the liquid or solid to be heated and melted. It is placed on the stage assembly which is lowered by hand into the top of the furnace. The connecting rod is attached to the motor shaft by a bolt. The balance is swung out of the way and the long hangdown tube was inserted in furnace so that it is just above the crucible. The balance is then swung back into position. The cylindrical sample is attached to a long nichrome extension wire and lowered down the hangdown tube. Its length is such that the sample just extended out of the bottom of the tube. The top of the extension wire has a loop which attached to the

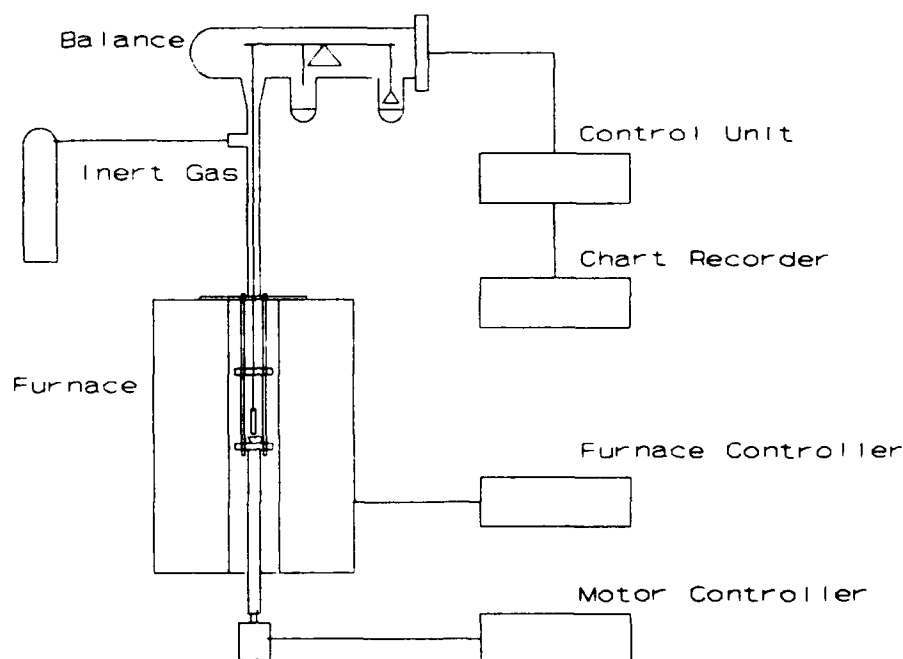


Figure 12 Schematic of apparatus for the immersion-emersion tensiometric method.

extension wire coming out of the vacuum bottle. The long hangdown tube is then raised so it is firmly mated with the vacuum bottle. The vacuum bottle assembly is lowered so that the sample is just above the liquid or solid in the crucible.

Next, the inert gas is allowed to flow into the furnace for approximately 10 minutes. Then the furnace temperature is raised to the desired operating level and the temperature is allowed to stabilize.

To begin a test, the chart recorder is turned on and for a wetting system the balance control unit is used to suppress the weight of the cylinder so that only the forces due to wetting are recorded. For a non-wetting system the weight of the cylinder is

suppressed such that recorder pen is at about 2/3 of the full scale. This way the reduction in downward force that occurs can be recorded.

The motor controller is set at the desired voltage i.e. speed. Upward motion of the liquid is started. When contact is made with the cylinder a change in force is noted. When the increase or decrease in force establishes a clearly linear response the motion of the bath is reversed and allowed to continue until the cylinder breaks free of the liquid and the balance reading returns to its original value. The chart recording is marked with the chart speed and motor voltage for later analysis.

This exact settings required for the apparatus are found by experimentation. Careful measurements are required so that the long hangdown tube is just above the crucible and the cylinder hangs just above the liquid. The choice of hangdown ports is dependent on sample size and the wetting forces as is the full range scales selected on the balance control unit and the chart recorder.

Care must be taken when handling the balance, hangdown tubes, extension wires, and sample to avoid the build up of static electricity which causes the extension wires and sample to stick to the sides of the hangdown tube. The vacuum bottle and hangdown tubes can be cleared of static electricity by rinsing them in acetic acid.

IV. EXPERIMENTAL RESULTS AND DISCUSSION

A. INTERMETALLIC FORMATION

1. Liquid Solder

Figure 13 shows the dissolution rate, dR_{eff}/dT , of Cu wires and Cu_6Sn_5 coupons in a liquid bath of 100% Sn. The dissolution rate of the Cu_6Sn_5 decreased with time while for Cu it remained relatively constant. Both rates increased with increasing bath temperature. In general, the dissolution rate of the Cu_6Sn_5 was higher than the Cu.

Figure 14 shows the same dissolution data as a function of average per cent weight of dissolved Cu in the tin bath. The baths used for the Cu_6Sn_5 coupons had a much more dissolved Cu than the ones used with the Cu wires. This was because the Cu_6Sn_5 were much larger than the Cu wires. The probable cause for the decline of the dissolution rate of the Cu_6Sn_5 was the progressive saturation of the Sn bath with copper. The difference in the dissolution rates between the Cu_6Sn_5 and the Cu increased with temperature. There appears to be a critical Cu concentration of the bath after which a decline in the dissolution rate of Cu_6Sn_5 occurs. This value is approximately 0.1 to 0.3 %weight of copper in the bath. This critical concentration is not seen for the Cu wires because the amount of dissolved Cu in the bath was much less.

Figure 15 is a plot of the dissolution rate as a function of time. For this experiment the solder baths were changed after dipping each sample to ensure the amount of Cu in the bath was kept to a minimum. The baths were 100% Sn at 270°C. Both

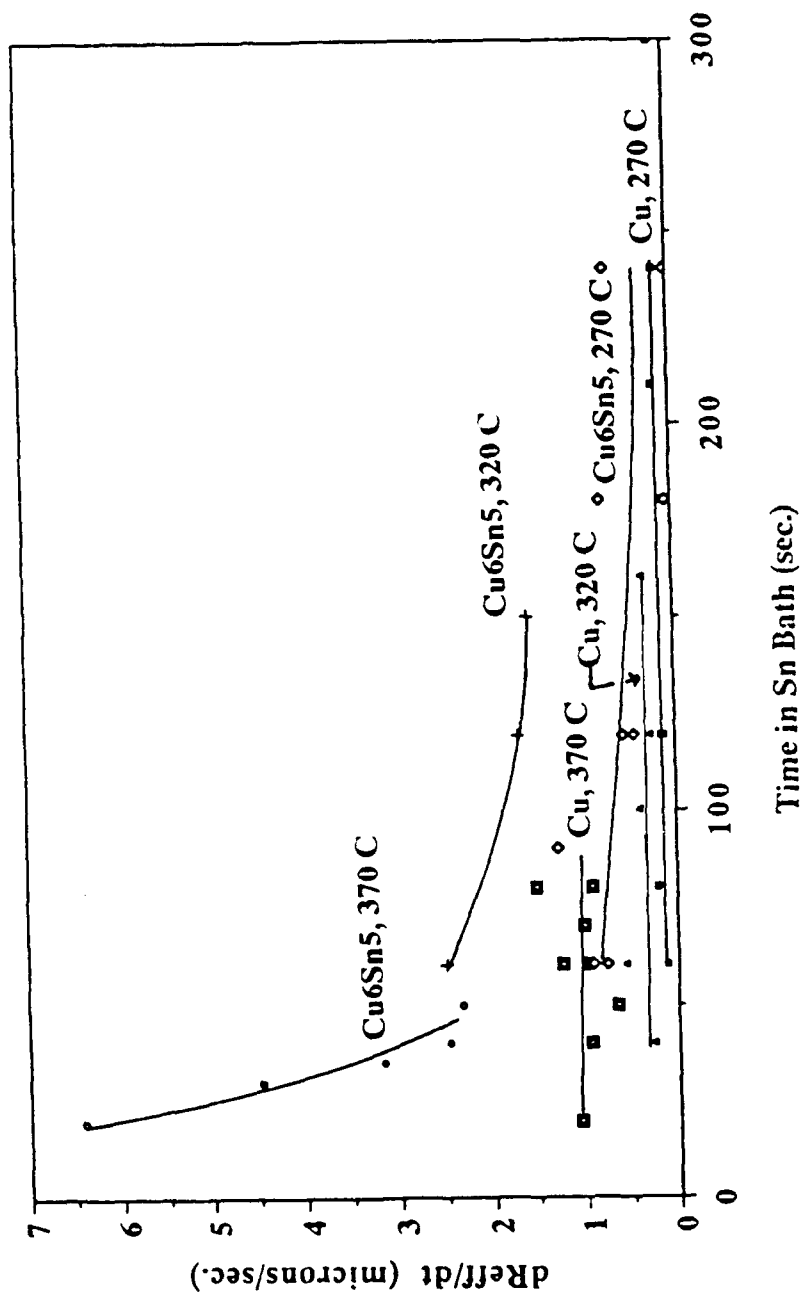


Figure 13 Comparison of dissolution rates as a function of time immersed in a 100% tin bath.

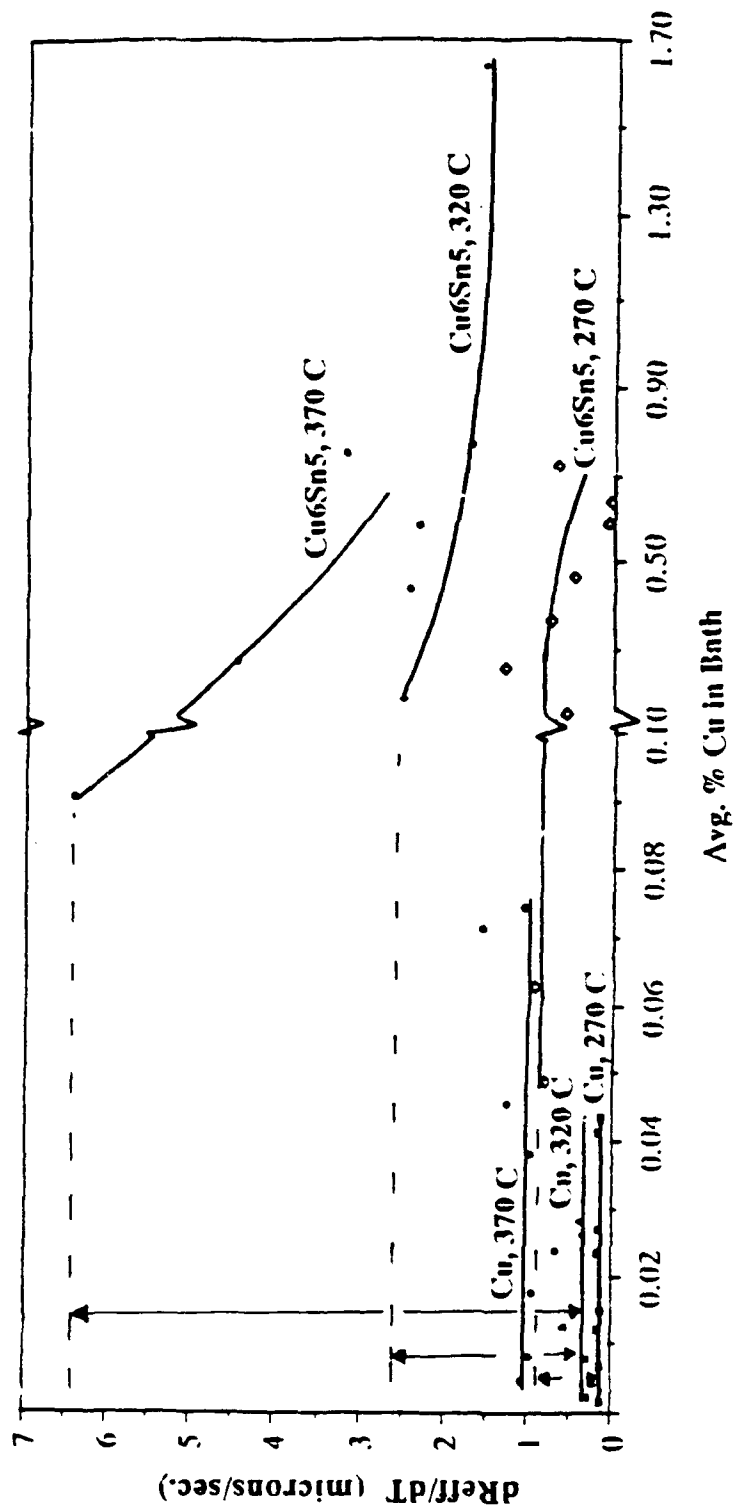


Figure 14 Comparison of dissolution rates as a function of the average concentration of copper dissolved in a 100% Sn bath.

dissolution rates were relatively constant with the rate for the Cu_6Sn_5 being over five times larger than the rate of the Cu. Earlier it was shown that the effective dissolution rate was accurate for comparisons of the two specimen sizes within a factor of two. Therefore, it is reasonable to assume that the dissolution rate of the Cu_6Sn_5 is significantly faster than the dissolution rate of the Cu.

Figure 16 shows the thickness of the intermetallic formed on the copper wires as a function of time. The error bars represent the range of thicknesses recorded for each specimen. This was necessary because growth was non-uniform and the value of thickness reported are averages. In general thickness increased with temperature and time. This is in spite of the fact that the dissolution of the Cu_6Sn_5 was shown to be greater than that of Cu. Around 80 seconds at the highest temperature (370°C), however, an apparent drop in the intermetallic thickness was noted. This datum needs to be verified in future experimental work.

Figure 17 shows two representative cross-sections of the copper wire with intermetallic growth on the surface. The specimen dipped at the lower temperature shows more uniform, planar growth. The specimen dipped at the higher temperature shows more irregular growth. Energy dispersive x-ray (EDX) analysis revealed impurities ahead at the intermetallic/unreacted tin interface. Silicon in particular was noted.

Figures 18 and 19 show the surface morphology of the Cu_6Sn_5 on two copper wire specimens. The Cu_6Sn_5 grows with time. At short times rounded protrusions of growth are seen. As time increases there is columnar growth of the protrusions. At the higher temperature and longest time (Figure 19) there is clearly faceted growth. This

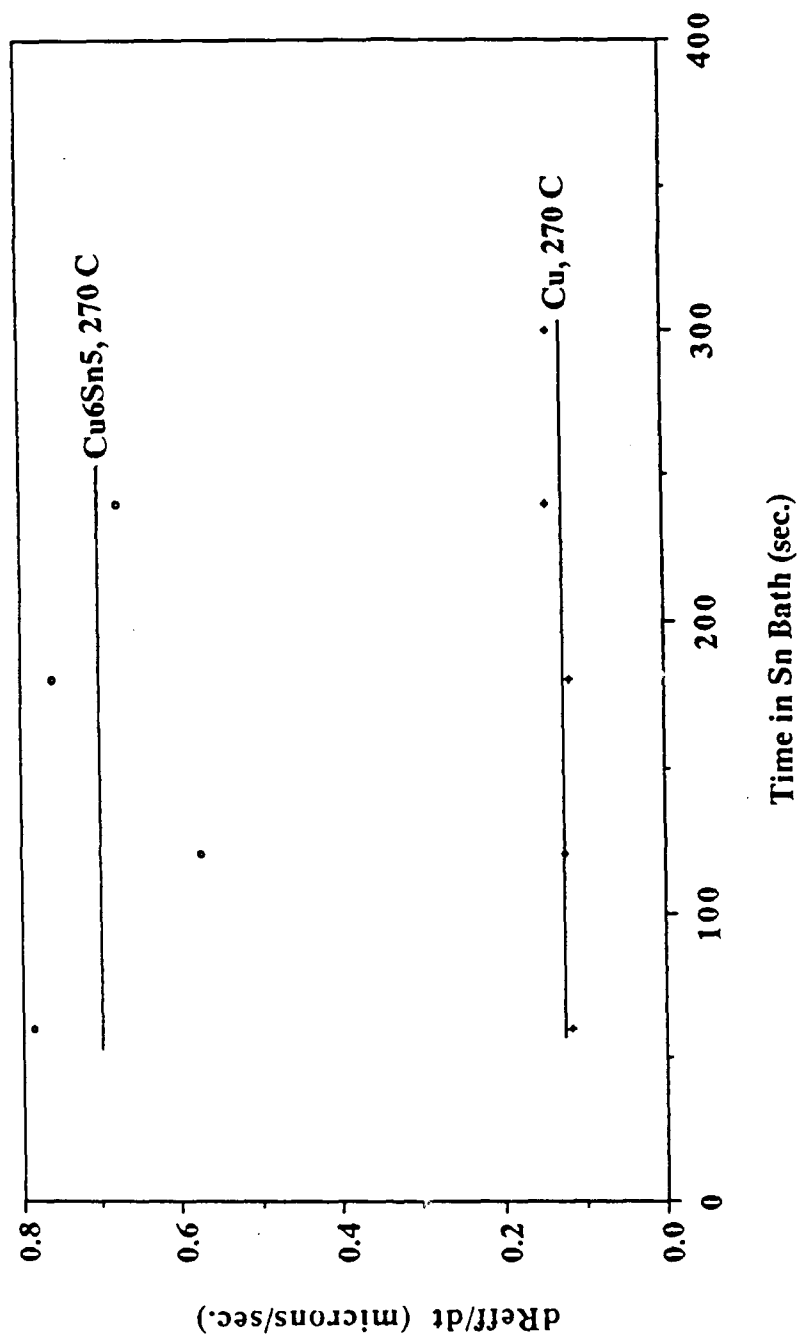


Figure 15 Comparison of dissolution rates in a 100% tin bath at 270°C with the concentration of dissolved copper in the bath kept to a minimum.

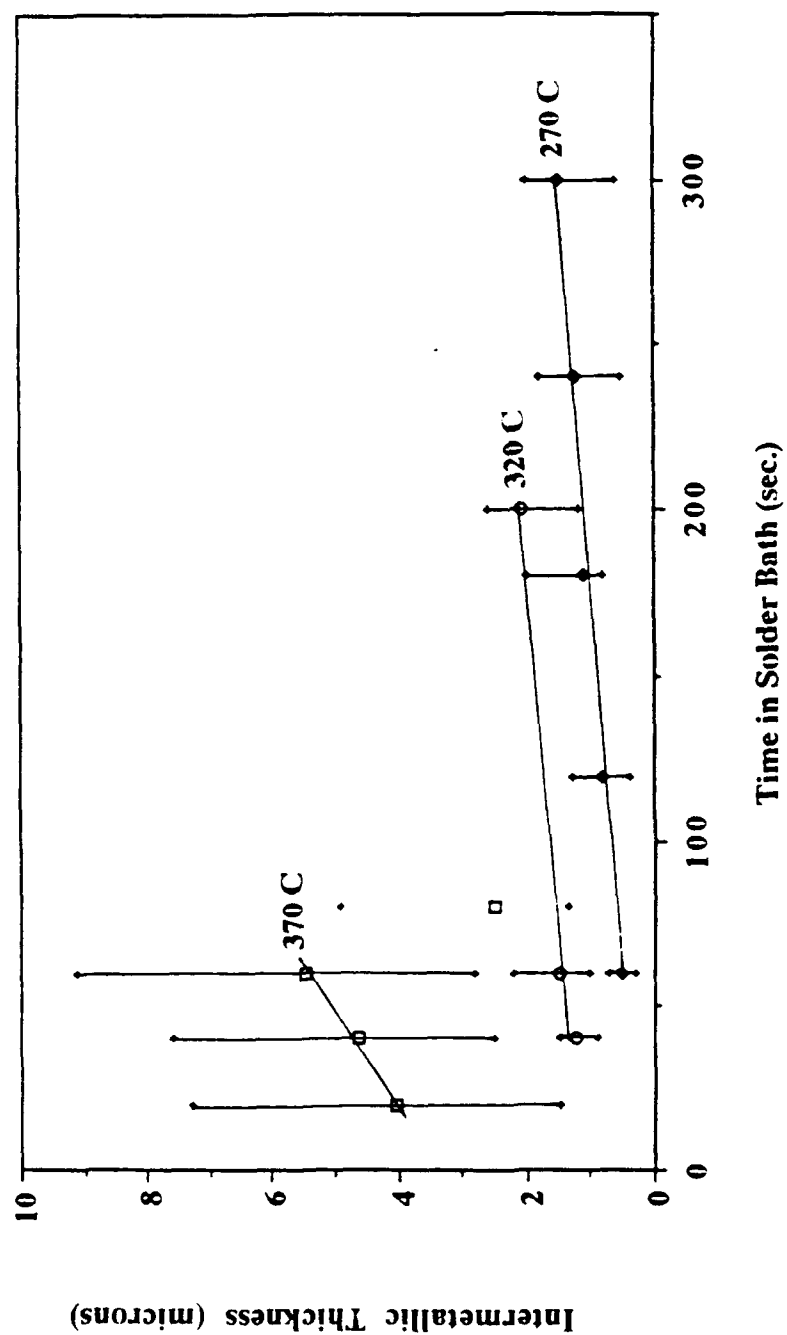


Figure 16 Intermetallic thickness formed on copper wires in 100% tin solder as a function of time.

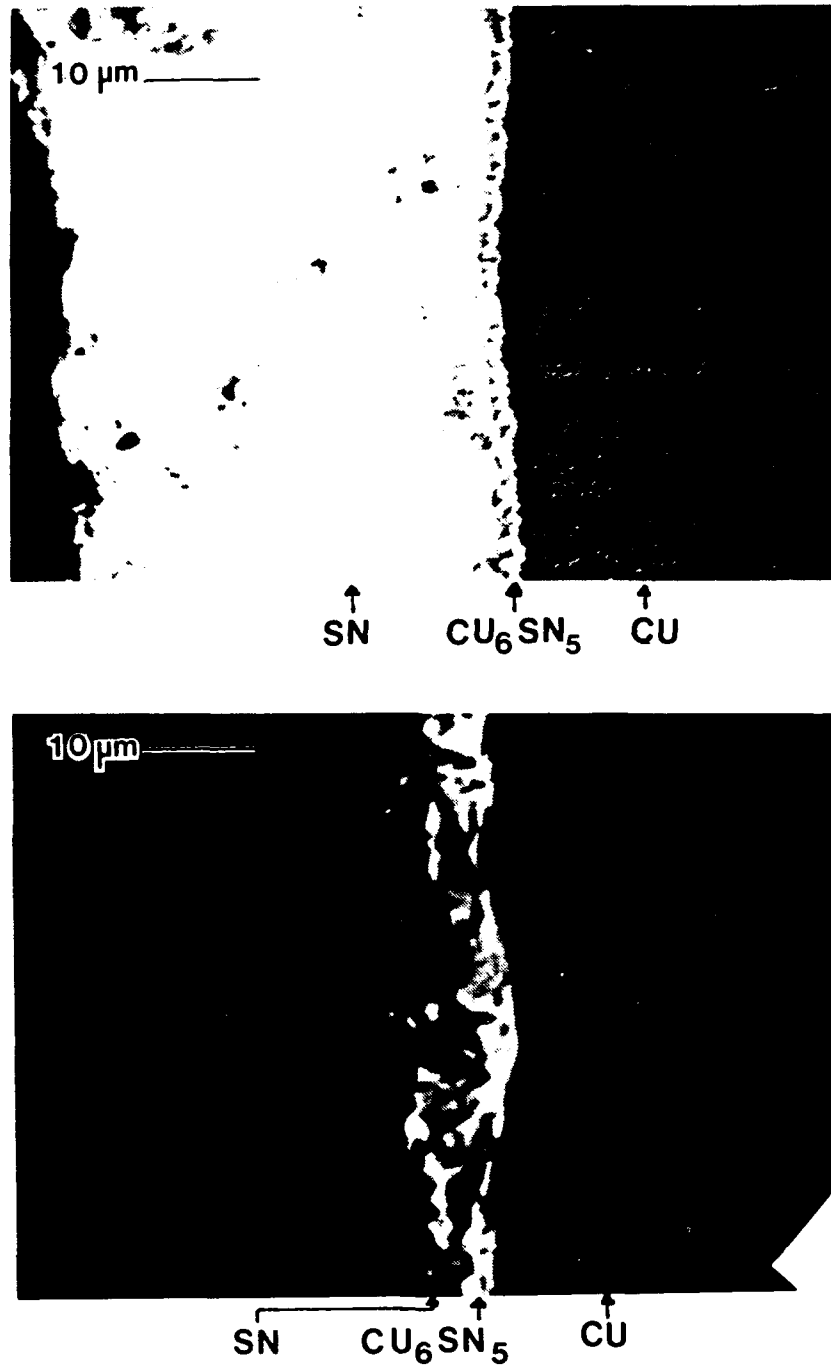


Figure 17 Irregular intermetallic growth on a copper wire. Both specimens were dipped in a 100% tin Bath. Top: 270°C for 60 seconds. Bottom: 370°C for 80 seconds.

faceted growth may be the reason there was such a large range of intermetallic thicknesses observed in Figure 16. The faceted growth is indicative of preferential growth along certain planes of the intermetallic crystal, typically those with low Miller indices. Faceted growth typically occurs when the rapid growth of high index planes relative to the low index planes makes only low-index planes exist at the surface [Ref. 20: p. 319]. Since low index planes grow relatively slowly, it is possible that once faceted growth is established, the dissolution rate of the Cu_6Sn_5 becomes greater than the growth rate, thereby resulting in a reduction in the total intermetallic thickness. This might explain the decrease in intermetallic thickness observed at long times at 370° (Figure 16).

Figure 20 compares the dissolution rates of Cu_6Sn_5 and Cu in a 100% Sn bath and in a 61.9Sn-38.1Pb bath. The dissolution rates of both Cu_6Sn_5 and Cu decreased with the addition of lead to the bath. The same decrease in the dissolution rate of the Cu_6Sn_5 with the increase in the concentration of Cu in the bath was noted.

2. Solid Tin

For comparison, several copper wires were dipped in a 100% tin bath for 20 seconds and then aged for two, four, and six days at 214°C , 20° less than the melting temperature of tin.

Figure 21 is a plot of intermetallic thickness as a function of time. The individual phases were not measured separately. This provided comparison with the solid-state ageing process. The thickness increased with time and on the specimen aged

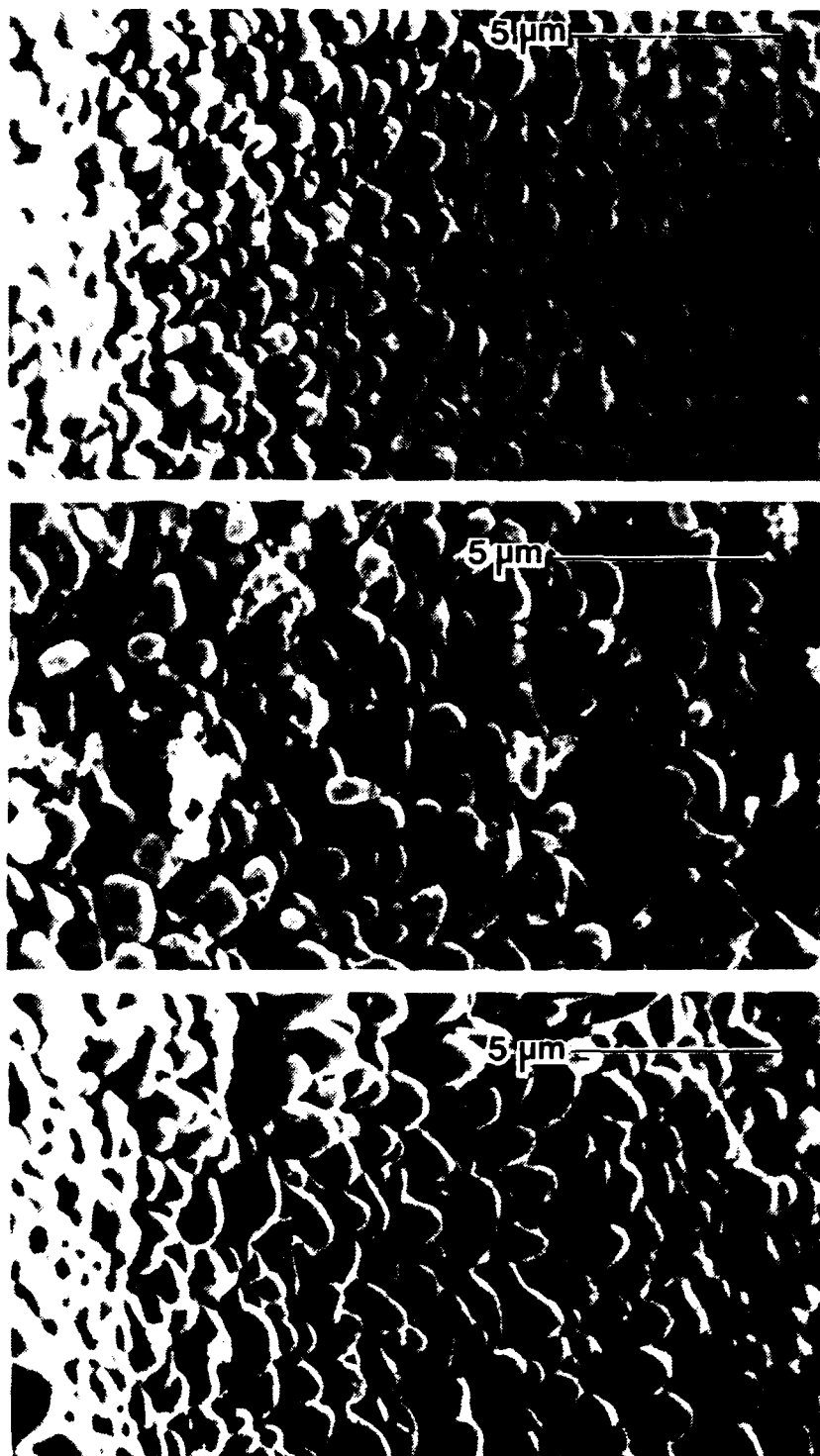


Figure 18 Surface of Cu_6Sn_5 on copper wire dipped in a 100% tin bath at 270°C for 40, 80, and 120 seconds.

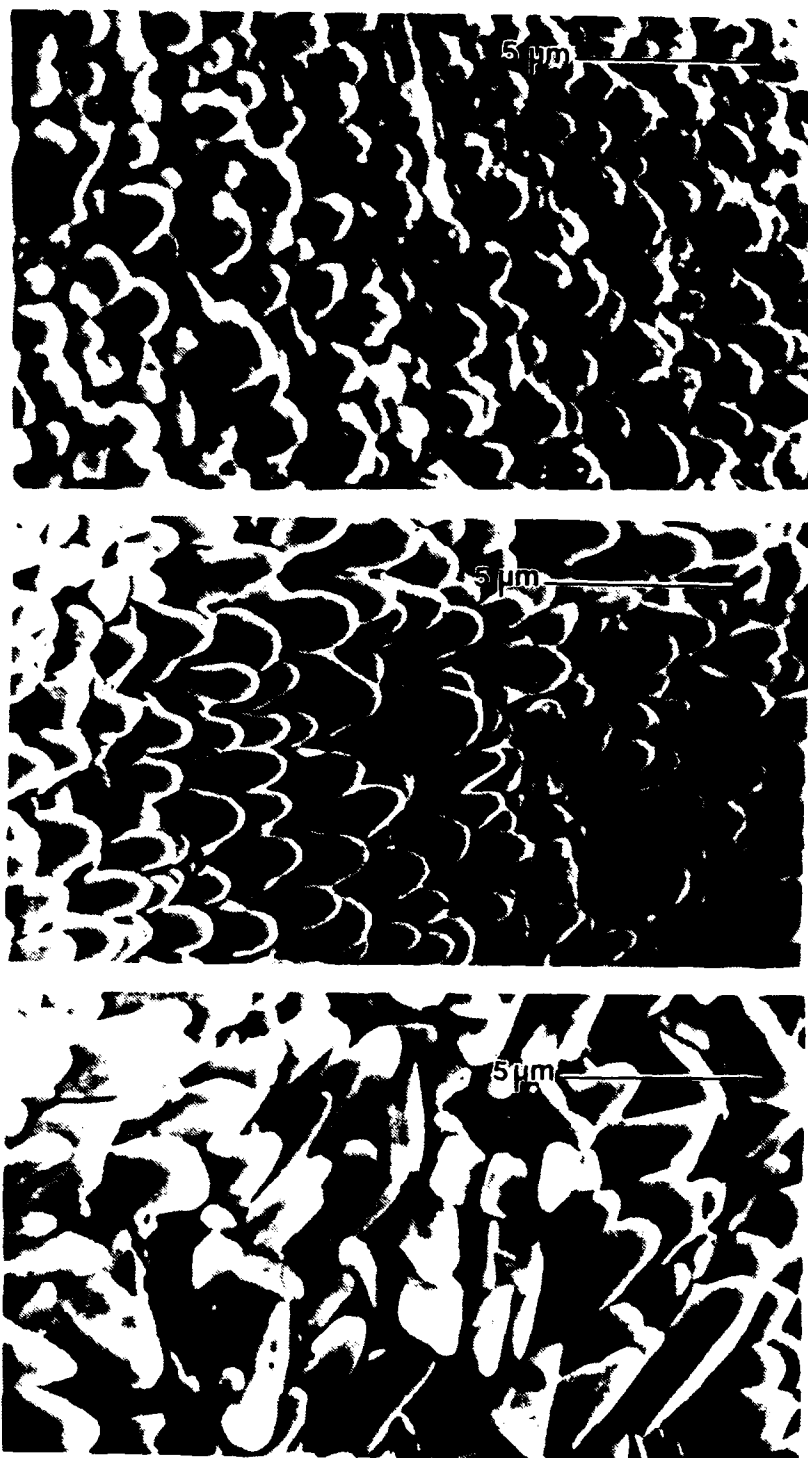


Figure 19 Surface of Cu_6Sn_5 on copper wire dipped at 370°C for 50, 70, and 80 seconds.

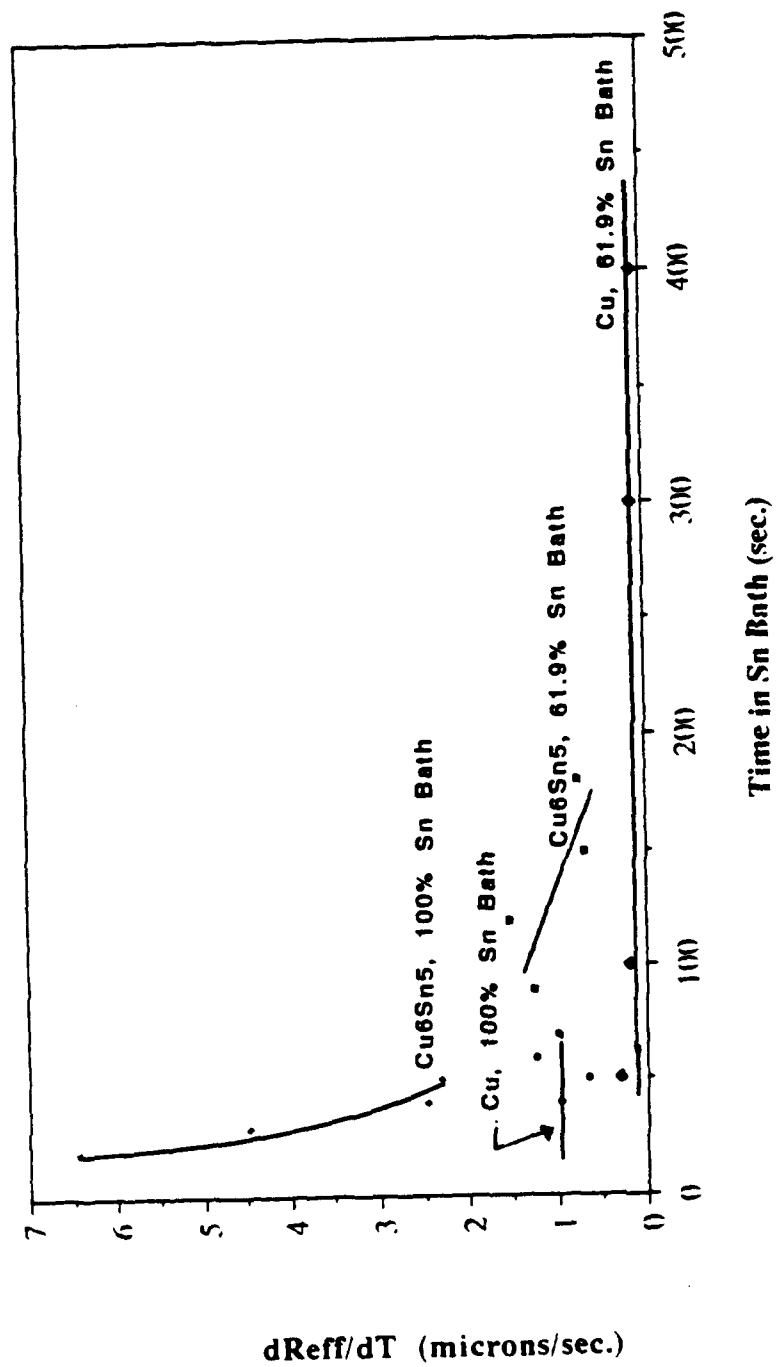


Figure 20 Comparison of dissolution rates in the two bath compositions at 370°C.

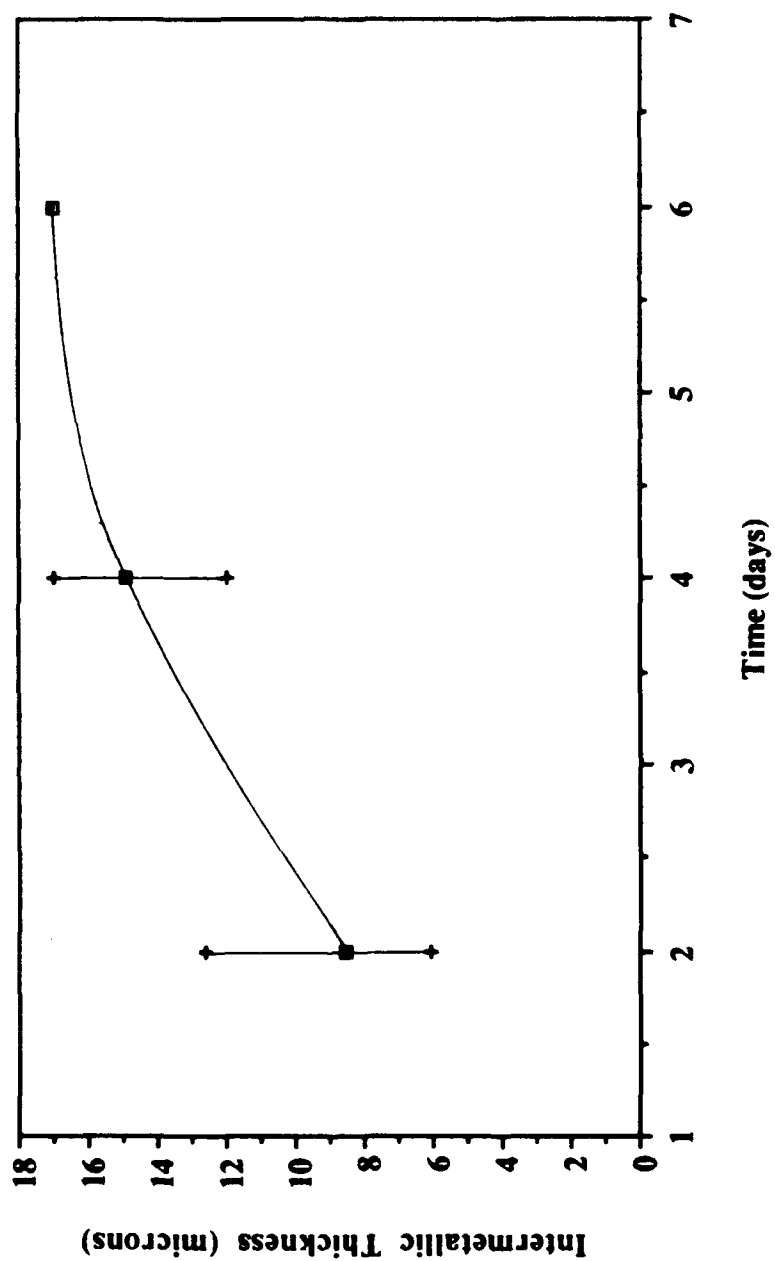


Figure 21 Intermetallic thickness as a function of time. Copper wire specimens were aged at 214°C.

six days all of the pure Sn had been converted to intermetallic. The error bars represent the range of thicknesses observed.

Figures 22 and 23 show the cross-section of the copper wires aged two and four days. The irregular thickness of the intermetallic is clearly visible. After two days the intermetallic was principally Cu_6Sn_5 . After four days both Cu_6Sn_5 and Cu_3Sn are present and after six days the intermetallic was primarily Cu_3Sn .

3. Review of Results

Analysis of the data collected shows the dissolution rate of the intermetallic compound was clearly greater than the copper yet in all but one case an intermetallic layer was not only observed but found to grow with time in the solder bath and temperature. The results of this study indicate that any intermetallic compound layer should diffuse into the liquid solder faster than it can form from the available copper. Furthermore, examination of the surface morphology of the Cu_6Sn_5 showed apparent growth with increased immersion time. Again, this seems in conflict with the results of the dissolution rate data.

One hypothesis is the rate of formation of the intermetallic compound is very fast when liquid tin is in contact with the solid copper. Once the intermetallic has formed its subsequent growth may be slower. This growth would be controlled by the rate of diffusion of copper and tin into the intermetallic, not the diffusion of copper into liquid solder. This rate of growth may be slightly faster than the rate of dissolution of the intermetallic in the liquid solder. The results from this study did not produce the first and



Figure 22 Tin coated copper wire aged 2 days at 214°C. The intermetallic is mostly Cu_6Sn_5 .

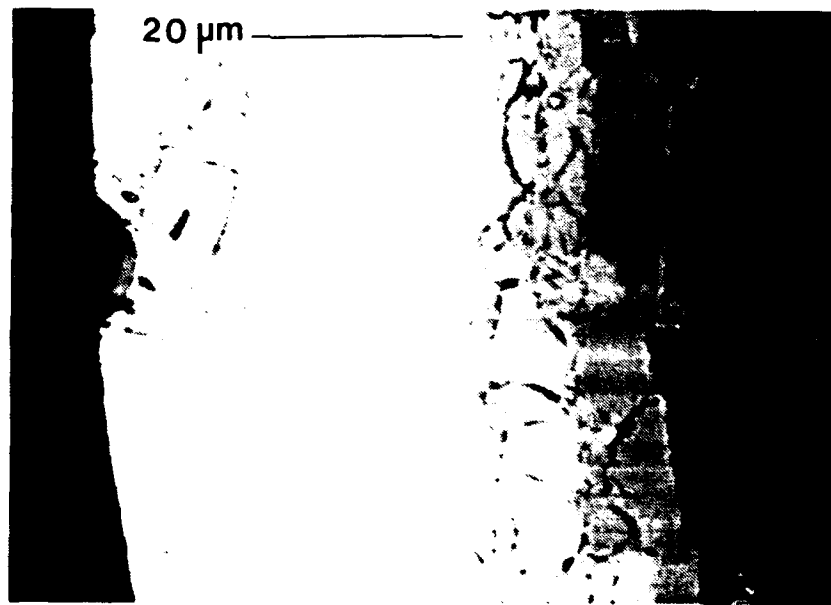


Figure 23 Tin coated wire aged 4 days at 214°C.

last stages of intermetallic growth noted by Kang and Ramachandrar. [Ref. 11: pp. 421-422]. The likely reason is the dipping times were too long to get the first stage and the solder baths too large in comparison to the copper wires to get the last stage. They did show the slow growth due to the competition between intermetallic growth and dissolution. It was also seen that the rate of intermetallic dissolution in the solder bath reduces dramatically when the bath becomes saturated.

The results of the specimen dipped in the 370°C bath for 80 seconds are markedly different from all others. Here faceted growth was clearly evident and the intermetallic thickness was much less than the shorter times at 370°C. A possible explanation is the dissolution rate of the intermetallic is faster than the rate of growth

once faceting begins. This is because faceting is indicative of slower preferred growth on lower on lower energy planes.

A possible interpretation of these results based on comparison of the intermetallic thicknesses of Figures 16 and 21 might be that the temperature of the liquid solder and the soldering time are not be as important as the conditions after solidification when solid-state aging occurs. But it must be remembered that this study looked at extreme situations. The copper wires were in the liquid bath for a very long time in comparison to actual soldering conditions and they were aged in solid tin at a very high temperature the relatively small thickness of intermetallic formed in comparison to the solid-state growth.

B. WETTABILITY MEASUREMENTS VIA THE IMMERSION-EMERSION TECHNIQUE

1. Procedure

The apparatus described in the previous chapter was constructed and several test runs were made. Tests were made with copper-liquid solder and copper-lubricating oil systems. Theoretically, both of these are wetting systems. A non-wetting system was not tested. Several experimental difficulties were encountered.

It was determined that for studying liquid metal-solid interfaces, special attention needs to be paid to the prevention of oxide formation. Fluxing the surface of the solid was not very effective because it sublimated long before the test was actually run. Nor was flooding the furnace and liquid surface with inert gas. The liquid solder

did not wet the solid copper in the tests performed. The tests with the oil and solid copper, however, were successful and were utilized to validate the experimental technique.

2. Test Results

In spite of the oxidation problem, it was desired to test the operation of the apparatus. For this reason a copper-lubricating oil system was used. The oil was HE-200 rotary pump oil produced by Joel U.S.A. Inc. Since no heating was required oxidation of the copper would be minimal.

Figure 24 is the strip chart recording of the test run. The test settings on the equipment were:

Balance range: 100 milligrams

Recorder Speed: 2 in./sec.

Motor voltage: 19 volts

The following points can be identified on Figure 25. At point A, the force is equal to the weight of the solid copper cylinder. By convention, force is set at zero at this value since it is constant. At point B, the solid contacts the oil and wetting is almost instantaneous. The increase in force is due to the weight of the meniscus on the cylinder. From B to point C, the decrease in force is due to the upward force of buoyancy countering the weight of the meniscus. The vertical motion of the oil bath is reversed at point C and emersion begins. From point C to point D, the upward force of buoyancy decreases as the cylinder pulls out of the oil. Though the bottom of the cylinder is clear of the level surface of the oil at point D, the meniscus hangs on the cylinder causing the downward force to continue to rise. At point E, the necking of the

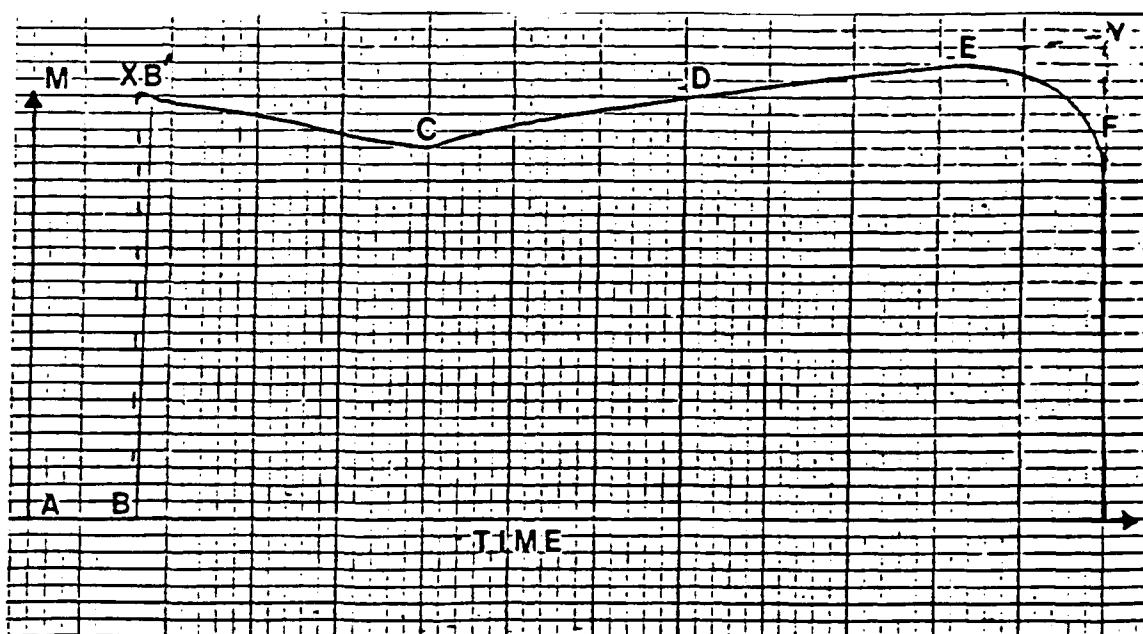


Figure 24 Strip chart recording from a test of a copper-lubricating oil system.

meniscus, negative joining angle, ϕ , causes the downward force to decrease. At point F, the meniscus falls off the cylinder.

Notably missing from this chart recording is the clear distinction of the linear and non-linear portions of the theoretical charts presented earlier. Close examination shows these regions to be very small. These non-linear portions are caused during the finite amount of time it takes for the instantaneous joining angle, ϕ , to reach the steady state immersion or emersion contact angles, θ_i and θ_e .

The surface tension, σ_{LV} , was determined using the maximum force recorded.

This was 27 mg at Point G. Using equation (15) of Chapter II:

$$\sigma_{LV} = \frac{F_{\max}^{\exp}}{p}$$

where $p = \pi \cdot D = \pi \cdot 0.0025 \text{ m} = 7.854 \cdot (10)^{-3} \text{ m}$. Therefore, $\sigma_{LV} = 3.37 \cdot (10)^{-2} \text{ N/m}$.

This compares favorably with the surface tension of SAE 30 oil which is $3.5 \cdot (10)^{-2} \text{ N/m}$.

The immersion and emersion contact angles, θ_i and θ_e , were then computed from points X and Y on Figure 24 using the following to equations introduced in Chapter II:

$$\theta_i = \arccos\left(\frac{F_{xg}}{\sigma_{LV} p}\right)$$

$$\theta_e = \arccos\left(\frac{F_{yg}}{\sigma_{LV} p}\right)$$

where:

$$F_x = 0.0248 \text{ Kg.}$$

$$F_y = 0.0280 \text{ Kg.}$$

Therefore, $\theta_i = 23.3^\circ$ but the value of θ_e was undefined.

Given that the Figure 24 differed in shape from the shape of curve for the wetting case proposed by Rivollet, Figure 5 of Chapter II and that θ_e was undefined when

calculated using the Rivollet's method of determining contact angles further analysis was required. In fact, Rivollet's work dealt almost exclusively with non-wetting systems and the immersion-emersion technique was validated with non-wetting systems [Ref. 12]. The wetting case was little more than a side note and actually determining the contact angles for it was not specifically discussed.

The shape of Figure 24 agrees with the shape of a similar force as a function of depth of immersion plot obtained by Chatain for a wetting system (Figure 25) [Ref. 17: p. 572]. Therefore, it is reasonable to expect that the Figure 24 is a valid result for the copper-lubricating oil system.

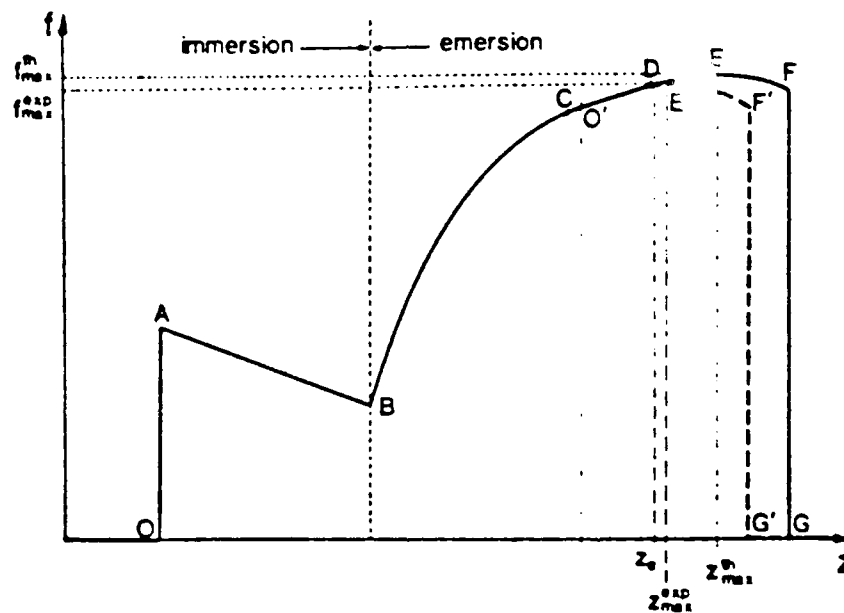


Figure 25 Force on the solid as a function of depth of immersion, z [Ref 17: p. 572]

According to Rivollet, the immersion and emersion contact angles are found from the force versus immersion depth curve. Specifically, at the points where the force

due to buoyancy is zero and therefore the force on the curve is solely due to the weight of the meniscus, W_m . As described in Chapter II, $W_m = \sigma_{LV} p \cos \phi$. The method of finding these points is illustrated in Figure 4 of Chapter II. The variation in the values of force represented by line segments CD and EF is due to the linear increase or decrease of the force due to buoyancy. The force due to the weight of the meniscus is constant during these periods. The value of the force at any point is:

$$F = \sigma_{LV} p \cos \phi + \Delta \rho g z s$$

Along CD and EF, $\phi = \theta_i$ and θ_e , respectively. The goal is to find the point along these lines where $z = 0$. This is the force due only to the weight of the meniscus. This is done by extending the lines to the vertical lines where $z = 0$. The intersection of the two lines is the force desired. With these two forces θ_i and θ_e can be calculated.

Applying this theory to the wetting system's curve obtained in this study shows that while the logic applies for determining θ_i it is incorrect for θ_e . This is because during emersion the point where the force due to buoyancy is zero does not correspond to the vertical line where the total force on the solid is zero as is the case with the non-wetting system. To determine θ_e for the wetting system the point where both $\phi = \theta_e$ and the force is due only to the weight of the meniscus must be found.

Using Rivollet's model of the wetting system, this would correspond to point E of Figure 24. At this point the volume of solid in the liquid is essentially zero but the liquid is still attached to the cylinder and the meniscus has not yet begun to neck.

If this analysis is applied to any wetting system, the point during emersion when both $\phi = \theta_c$ and the force recorded is due only to buoyancy occurs where the linear portion of curve ends. At this point the increase in force is no longer due to the linearly declining, upward buoyancy force. After this point the meniscus begins to "stretch" causing added force downward. Using this analysis, θ_c of the copper-lubricating oil system was calculated to be 22.2° based on a force of 0.025 Kg.

Figure 26 is a summary of the progressive steps in the force vs. immersion depth curve obtained in this study. Each of the steps is explained below. The force on the solid is abbreviated F, the weight of the solid, W_o , the weight of the meniscus, W_m , and the force due to buoyancy, B.

Point 1: $F = W_o = 0$, by convention.

Point 2: Cylinder touches surface of the liquid and wetting is almost instantaneous. Between 2 and 3 ϕ goes to θ_i . This causes a non-linear decrease in force. The length of this transition period depends on the speed of wetting. In this study wetting was very fast and the non-linear portion is barely observable. With other systems it may be more pronounced.

Point 3: As cylinder lowers into the liquid, $\phi = \theta_i$ and the upward acting B increases linearly while W_m is constant. Therefore, F decreases linearly.

Point 4: Direction of cylinder travel is reversed and emersion begins. Again, θ_i must go to θ_c and there will be a transition period where the change in force is non-linear.

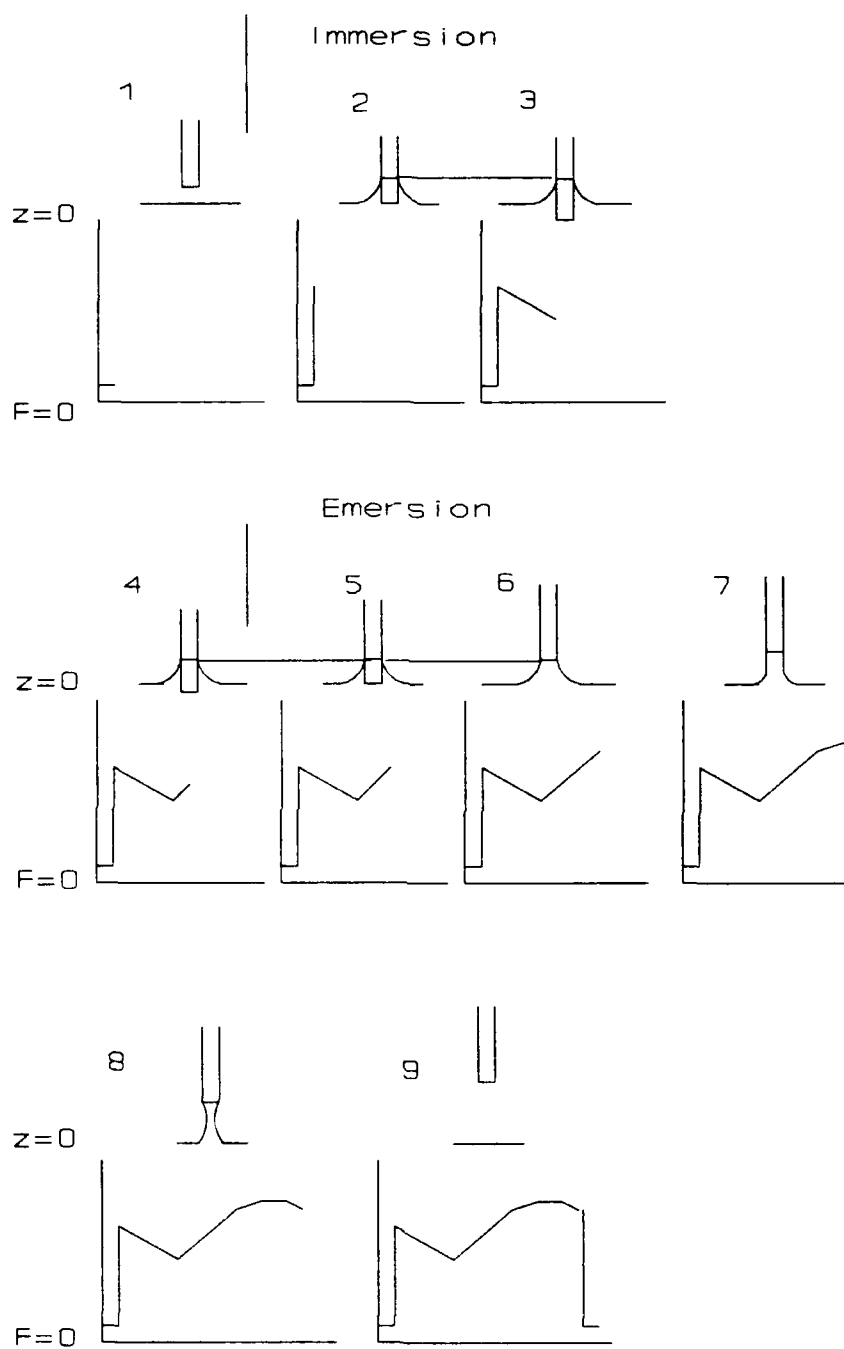


Figure 26 Schematic of the progressive steps of the immersion-emersion test of a wetting system.

Point 5: $\phi = \theta_c$ and B decreases linearly while W_m remains constant.

Therefore, F increases linearly.

Point 6: Volume of the cylinder in the liquid is zero yet the meniscus hangs on to the cylinder. $B = 0$ and $F = W_m$. This is the force used to calculate θ_c .

Point 7: Raising cylinder pulls the meniscus up with it. W_m increases and it is maximum when $\phi = 0$.

Point 8: Meniscus begins to neck causing W_m to decrease and therefore F decreases.

Point 9: Meniscus falls off the cylinder and F returns to W_0 .

Table II shows the results obtained for the oil-copper system.

Table II Results of the immersion-emersion test of the oil-copper system.

Oil-Copper System	
σ_{LV} (N/m)	3.37×10^{-2}
θ_i	23.3°
θ_c	22.2°

Calculation of Young's contact angle, θ_Y , and the work of adhesion, W_a , was not possible because the Wenzel parameter, r , was not known for the copper rod. In future work it would be desirable to measure this value with the appropriate equipment.

V. CONCLUSIONS AND RECOMMENDATIONS

A. INTERMETALLIC FORMATION AND COMPETING RATES OF DISSOLUTION

This study examined two of the processes affecting the formation and growth of the intermetallic compound layer between molten solder and a copper substrate, the diffusion of copper and the diffusion of the intermetallic compound, Cu_6Sn_5 , into the liquid solder. Comparison was made of the relative dissolution rates. The goal was obtaining a greater understanding of the affects of initial soldering parameters on intermetallic compound formation.

The thickness of the intermetallic generally increased with time and temperature. The dissolution of copper in liquid solder was much slower than the dissolution of the intermetallic into the liquid solder yet the intermetallic compound grew. This was evidenced by the intermetallic thickness measurements made and the observations of the intermetallic's surface morphology. Based on these results and the findings of other researchers examining the nickel-tin system it is believed that initial growth is very fast and then it is reduced as the intermetallic diffuses into the solder bath and progressively saturates it. There exists a competition between intermetallic growth and dissolution. The intermetallic continues to grow but at a slower rate. The work of other researchers [Ref. 11] indicates that as the solder becomes saturated with copper the rate of intermetallic growth will increase. Also, establishment of faceted growth may decrease

growth rate to the extent that the dissolution rate becomes larger, resulting in a net decrease in intermetallic thickness at long times and high temperatures.

Future study could more generate more data to validate the hypotheses set forth here. A larger bath of liquid solder in non-silica crucible, such as graphite, is recommended. Similarly, it would be preferred to have copper and intermetallic specimens of the same dimensions.

B. IMMERSION-EMERSION TENSIO-METRIC TECHNIQUE

The goal of this part of the study was to construct and test the apparatus required to use the immersion-emersion method of determining contact angles. Construction and preliminary tests were conducted though numerous difficulties were encountered.

The apparatus was greatly affected by the build-up of static electricity. This accumulation was probably due to excessive amount of handling of the sample, the sample wire, and the hangdown tube required when mounting the sample. Also the balance was extremely sensitive to excessive force being applied to it. This would be easier to avoid if mounting the sample were easier.

Oxidation of the sample and the liquid bath was another problem encountered. The slight oxidation occurring made the testing of the solid copper and liquid tin system impossible. A better means of preventing oxidation is required.

All aspects of the apparatus worked well when testing the solid copper and lubricating oil system. The recorded plot of force as a function of depth of immersion was not exactly as predicted by the theoretical presentation in Chapter II, making the

determination of the emersion contact angle, θ_e , difficult. Based on the present results an alternate method of finding θ_e was proposed based on analysis of the dynamics of the forces involved during emersion. Further experimentation is required to completely validate the method for all systems of interest.

LIST OF REFERENCES

1. Klein Wassink, R. J., *Soldering in Electronics*, 2nd ed., Electrochemical Publications Ltd., 1989.
2. Thwaites, C. J., "The Attainment of Reliability in Modern Soldering Techniques for Electronic Assemblies," *International Metallurgical Reviews*, volume 17, 1972.
3. Davis, Paul E., Malcolm E. Warwick and Stephan J. Warwick, "Intermetallic Compound Growth and Solderability of Reflowed Tin and Tin-Lead Coatings," *Plating and Surface Finishing*, volume 70, August 1983.
4. Tribula, D., D. Grivas, D. R. Frear and J. W. Morris, Jr., "Observations on the Mechanisms of Fatigue in Eutectic Pb-Sn Solder Joints," *Journal of Electronic Packaging*, volume 111, June 1989.
5. Hagstrom, R. A. and R. N. Wild, in Proceedings of the Technical Programme, International NEPCON (National Electronic Packaging and Production Conference), Brighton, October 1969.
6. Parent, J. O. G., D. D. L. Chung and I. M. Bernstein, "Effects of Intermetallic Formation at the Interface Between Copper and Lead-Tin Solder," *Journal of Materials Science*, volume 23, 1988.
7. Tu, K. N. and R. D. Thompson, "Kinetics of Interfacial Reaction in Bimetallic Cu-Sn Thin Films," *Acta Metallurgica*, volume 30, May 1982.
8. DeHaven, P. W., IBM Internal Report IBM-EF-52, 1984.
9. Zakraysek, Louis, "Intermetallic Growth in Tin-Rich Solders," *Welding Research Supplement*, volume 51, 1972.
10. Warwick, M. E. and S. J. Muckett, "Observations on the Growth and Impact of Intermetallic Compounds on Tin-Coated Substrates," *Circuit World*, volume 9, number 4, 1983.
11. Kang, S. K. and V. Ramachandran, "Growth Kinetics of Intermetallic Phases at the Liquid Sn and Solid Ni Interface," *Scripta Metallurgica*, volume 14, 1980.
12. Rivollet, I., D. Chatain and N. Eustathopoulos, "Simultaneous Measurement of Contact Angles and Work of Adhesion by the Immersion-Emersion Technique," *Journal of Materials Science*, volume 25, 1990.

13. Davis, Paul E., Malcolm E. Warwick and P. J. Kay, "Intermetallic Growth and Solderability," *Plating and Surface Finishing*, volume 69, September 1982.
14. Laurent, V., D. Chatain, C. Chatillon and N. Eustathopoulos, "Wettability of Monocrystalline Alumina by Aluminum Between Its Melting Point and 1273 K," *Acta Metallurgica*, volume 36, number 7, 1988.
15. Rivollet, I., "Contact Angles and Thermodynamic Adhesion with Non-Reactive Metal-Alumina Systems," Dissertation, INP Grenoble, 1988.
16. Orr, Jr., F. M. and L. E. Scriven, "Menisci Around Plates and Pins Dipped in Liquid: Interpretation of Wilhelmy Plate and Solderability Measurements," *Journal of Colloid and Interface Science*, volume 60, number 2, June 15, 1977.
17. Chatain, D., L. Martin-Garin and N. Eustathopoulos, "Experimental Study of The Liquid-Liquid Interfacial Tension of a Ga-Pb System at The Monotectic Temperatures," *Journal de Chimie Physique*, volume 79, 1982.
18. Bader, W. G., "Dissolution of Au, Ag, Pd, Pt, Cu and Ni in a Molten Tin-Lead Solder," *Welding Research Supplement*, December 1969.
19. *Metals Handbook*, volume 13, American Society for Metals, 1985.
20. Flemings, Merton C., *Solidification Processing*, McGraw-Hill, Inc., 1974.

INITIAL DISTRIBUTION LIST

- | | | |
|----|---|---|
| 1. | Defense Technical Information Center
Cameron Station
Alexandria, Virginia 22304-6145 | 2 |
| 2. | Library, Code 52
Naval Postgraduate School
Monterey, California 93943-5002 | 2 |
| 3. | Professor I. Dutta, Code ME/Du
Department of Mechanical Engineering
Naval Postgraduate School
Monterey, California 93943-5000 | 1 |
| 4. | Research Administration, Code 012
Naval Postgraduate School
Monterey, California 93943-5000 | 1 |
| 5. | Raymond Martin
121 Bayberry Lane
Westport, Connecticut 06880 | 2 |
| 6. | Department Chairman, Code ME/Hy
Department of Mechanical Engineering
Naval Postgraduate School
Monterey, California 93943-5000 | 1 |
| 7. | Naval Engineering Curricular Office, Code 34
Naval Postgraduate School
Monterey, California 93943-5000 | 1 |
| 8. | Mr. K. Hoffer
Naval Weapons Support Center
Code 6043
Crane, Indiana 47522 | 1 |